Aalborg University

Multi agent wireless systems

Wireless Communication Systems 10

Characterization of Dynamics of the User influence For Mobile Phone Antenna

Supervisor:
Gert Pedersen
Alexandru Tatomirescu
Emil Buskgaard

Authors:
Maria Mateva
Simon Stanev

June 4, 2014

AALBORG UNIVERSITY

Department of Electronic Systems
Electronic Engineering
Fredrik Bajers Vej 12
9220 Aalborg Ø
Telefon 99 40 86 00
http://es.aau.dk

Title:
Characterization of Dynamics of the User influence For Mobile Phone Antenna

Subject:
Multi agent wireless systems

Project period:
WCS 10, Spring semester 2014

Group:
Group 1055

Authors:
Maria Mateva
Simon Stanev

Supervisors:
Gert Pedersen
Alexandru Tatomirescu
Emil Buskgaard

Copies: 9

Page count: 75

Appendix: 5

Completed: XXXX, 2013

Synopsis:

This project summarizes the challenges associated with antenna design for a smart phone.A handset antenna has to be embedded in a smart phone without sticking out of the profile of the smart phone and this leads to a tremendous challenge for antenna designers.In addition these antenna have to operate in multiple bands according to world wide standards.The focus on this thesis is designing, manufacturing ,measuring electrically small antennas, introducing MIMO and investigating what is the influence on the parameters of the handset antennas when it is in close proximity to human body. Moreover, an RF cable feeding the antenna will degrade the performance of the antenna and this effect has to be minimized as much as possible.

Contents

List of Abbreviations

1G First Generation

2G Second Generation

3G Third Generation

4G Forth Generation

5G Fifth Generation

AA Antenna Array

AF Array Factor

BS Base Station

BW Bandwidth

CST-MS Computer Simulation Technology-Microwave Studio

ECC Envelope Correlation Coefficient

FSPL Free Space Path Loss

HPBW Half-Power-Beamwidths

IFA Inverted F-Antenna

LOS Line of Sigh

LTE Long Term Evolution

MS Mobile Station

MW Microwaves

MIMO Multiple-Input Multiple-Output

NLOS Non Line of Sight

PCB Microwave Printed Circuit Boards

PIFA Planar Inverted F Antennas

RF Radio Frequency

SNR Signal to Noise Ratio

SMS Short Message Service

VSWR Voltage Standing Wave Ratio

VNA Vector Network Analyzer

MIMO Multiple Input Multiple Ouput

LTE Long Term Evolution

RF Radion Frequency

SAR Specific Abosrbtion Rate

HAC Hearing and compability

OTA Over the Air

GPS Global Positon System

MEG Mean Effective Gain

ICNIRP International Commission on Non-Ionizing Radiation Protection

FCC Federal Communication Commission

SAM Specific anthropomorphic mannequin

TRP Total radiated power

TIS Total isotropic sensitivity

EIRP effective isotropic radiated power

WWAN Wireless Wide Area Network

List of Figures

List of Tables

Chapter 1

Introduction

1.1 Introduction

The art of antenna design engineering is tremendous challenge since the mobile phones are not used only for real time speech and text message services but increasing number of applications such as games, camera, browsing the internet and you name it. This sets two main trends in antenna design one is the mobile handset antennas to be small, built-in and meet multiband demand. Second trend is antennas to be multistandard fulfilling all industry requirements such as Specific Abosrbtion Rate (SAR), Hearing and compability (HAC) and Over the Air (OTA)) [1]. The focus on this thesis is designing, manufacturing and measuring electrically small antennas that comply with all requirements of the nowadays mobile communication. New generation of high data services require not only multiband antennas but also high efficiency and low correlation between the elements, which is taken into account in the antenna manufacturing lifecycle. In mobile communication systems, the quality of the RF link between a base station and a mobile station strongly depends on the amount of power that is transmitted and received by the mobile station. The power depends, among other factors, on the mobile phone and antenna design. Moreover, the mobile phone is used in close proximity to a user's body, which reduces the transmitted and received power. The ratio of the power with and without the user's body is defined as body loss and it may vary depending on the antenna design.In the scope of the work is also investigating the mobile antennas when are in close proximity to human body. In this work important part is validating results from simulation and measurements, this requires additional familiarizing with CTIA test plans where is described how the user effect measurements to be done. Measurements of the free-space radiation characteristics of small antennas typically suffer from the influence of the attached cables. In this thesis part is devoted to analyzing those effect and design chokes for reducing those undesired effects.

1.2 Problem Description

This section aims to state the issues related to designing an antenna for Mobile Station (MS) , Radion Frequency (RF) cable effects on the characteristics of the antenna and interaction with the user's lossy tissue .

1.2.1 Issues related to designing an antenna for MS.

Three main problems will arise:

- Design of an antenna for a smart phone leads to limited space.
- The impedance of the antenna must be matched to dual frequency bands in order to cover all of the mobile phone standards. These bands will be stated in sec. 1.5 on page 5.
- High correlation between MIMO antenna elements

1.2.2 Issues related to cable effects .

The RF cable can affect the characteristics of the antenna as follows :

- Changing the input impedance.
- Current distribution on the outer shield of the RF cable can lead to spurious radiation and degradation of the radiation characteristics.
- In contrast to an antenna in free space the radiation characteristics will be different and this can be minimized by the use of a choke [2].

1.2.3 Issues related to user's interaction.

The human hand will effect the performance of the MS antenna:

- The input impedance will change dynamically depending on the grid style of the user.
- Presence of a human tissue near the mobile phone changes the input impedance of the antenna, which may either improve or degrade the antenna matching, thus changing the amount of radiated power.
- The user will absorb some of the emitted energy, which will change the radiation characteristics of the antenna.

1.3 Motivation

Nowadays the mobile communication require mobile phone to operate in diverse services communication services. A smart phone consists of many components in it, such as battery,display and touchscreen , memory, camera, speakers, processors and etc. All of these components drop off very little space in a smart phone. Supplementary, an antenna has to be embedded in the smart phone without sticking out of the profile of the smart phone and this leads to a tremendous challenge for antenna designers. In addition these antenna have to operate in multiple bands according to world wide standards. First, the motivation behind this project is to designed such an antenna. Two main types will be examined, which are monopole and Planar Inverted F Antennas (PIFA). These types of antenna are the most suitable for the purpose due to the fact that they are very compact, inexpensive to manufacture and at last but not least they show good characteristics. Second, the designed antenna will be simulated in Computer Simulation Technology-Microwave Studio (CST-MS) and measured with a Vector Network Analyzer (VNA) for impedance matching and the the radiation characteristics will be investigated in an anechoic chamber. Furthermore, it is well know that an RF cable feeding the antenna will degrade the performance of the antenna due to current distribution on the outer shield of the RF cable in comparison of an antenna place in an free space. Moreover this effect could be minimized significantly with a choke sleeve. Third, a Multiple Input Multiple Ouput (MIMO) will be applied, where an investigation will be done for spatially decorrelated antenna aiming for increasing the data rate. Finally, it will be studied what is the influence on the performance of the antenna with regards to the user's lossy tissue, such as the head and the hands.

1.4 Requirements

1.4.1 Genreal

In order an antenna to be used for cellular communication it has to fulfill some requirements. In tbl. 1.1 on the next page are shown the cellular frequency bands. Both operating bands Second Generation (2G) and the Third Generation (3G) are called Wireless Wide Area Network (WWAN) system [3]. These bands could be divided in general into low $698 - 960$ and high $1710 - 2690$ band.

Further more the following criteria has to be fulfilled:

- For the sake of matching the antenna to operate at the Bandwidth (BW)s shown in tab. 1.1 on the following page a certain level of threshold value of the reflection coefficient $S11 = -6dB$ is taken into account [4, 5, 3, 6].

Generation	Name of band	Frequency Range (MHz)
2G	GSM850	$824 - 894$
	GSM900	$880 - 960$
	PCS1800	$1710 - 1880$
	DCS1900	$1850 - 1990$
3G	UMTS2100	$1920 - 2170$
4G	LTE700	$698 - 787$
	LTE2300	$2305 - 2400$
	LTE2500	$2500 - 2690$

Table 1.1: *Frequency range of the cellular communication [3].*

- Considering the mutual coupling a threshold value of $S21 \leq -8dB$ will contribute to a lower Envelope Correlation Coefficient (ECC) when a MIMO or diversity is used [6, 7].
- An ECC ≤ 0.7 MIMO can achieve separate streams in favor of increasing the data rate [6, 7].

1.4.2 CTIA specifications

In the test plan for mobile station over the air Performance defined by CTIA are defined methods of measurement for radiated RF power and receiver performance. In the specification requirements are defined how the measurements of the user effect to be conducted. It's how the reuqirments for our simulation and measurements are set.
For simulation of devices less than 56 mm wide.

- Talk mode for the hand and head simulations
- The head and hand talk mode configuration specifies that the EUT is not in direct physical contact with the cheek of the phantom but tilted away from the cheek by an angle of 6^{o}, the acceptable error is +- 2 ^{o}.
- Index finger must press must press against the back, ring finger must be in contact at the bottom, middle finger should be also in contact, the pinky finger must not touch the casing and the thumb should be in touch with the EUT.
- Phone should be faced up, it should make 120 $^{\circ}$ angle with hand spacer

  For measurements of devices less than 56 mm wide.

- The side of the EUT shall be aligned against the side wall of the tool. The base of the EUT shall rest on the wide hump with ruled markings, and the flip of the EUT shall rest on the narrow hump.
- Position the conformal fold palm spacer in the fold hand phantom corresponding to the right-handed or left-handed configuration.
- Position the EUT in the Fold Hand Phantom, resting on the index fingertip and palm spacer, with the bottom of the EUT aligned to the ruling on the palm spacer that corresponds to the reading.
- Ensure all fingers are in contact with the EUT and spacer.

  For measurements of devices 56 to 72 mm wide.
- Measurements and simulation are done with the standard hand grip for devices 56 72 mm wide.
- Talk mode for the hand and head simulations
- EUT should be place on the hand spacer
- Side walls of the spacer must be aligned wth the phone
- If the EUT is shorter than 135 mm, then e top of the EUT must be aligned with the top of the hand spacer. Otherwise, align the bottom of the EUT with the bottom wall of the spacer.

1.5 Delimitations

This section will present the delimitations with respect to designing an integrated antenna for a smart phone , choke sleeve and at last user's interaction.

The following criteria are considered as delimitation factors for the antenna design:

- The antenna has to be impedance match to two wide operating bands $698 - 960$ MHz and $1710 - 2690$ MHz in order to cover all of the standards mentioned above.
- To implement such an antenna in a smart phone the antenna designer are restricted in space.In this project it is assumed that dimensions of such devices are 120x60x10 mm^3.In over all the maximum left cut back space for the an antenna is 10x60x8 mm^3 at the bottom and top side of the smart phone in order to provide MIMO to increase the data rate or diversity to improve the reliability of reception.
- ECC will be evaluated from the far-field of the antenna in CST-MS.

1.5.1 Choke design

NOT COMPLETED - DO NOT READ The choke is used to minimized the effect of the RF cable and two are the main delimitations considered for designing a choke:

- Simple structure for the sake of ease manufacturing.
- Thickness of the walls is 1 mm.
- Coaxial cable of radius 1 mm will be used in order not to bent under mechanical destruction.

1.5.2 User effect measurements

As mentioned in sec. 1.4 on page 3 there were two phantom models described for measuring devices with different width. This project will be limited only for talk mode where the users uses only one hand.There are the following criteria that have to be taken as limiting factors:

- Only hand and head phantohm for devices narrower than 56 mm is available for simulation sake.
- If the EUT is wider than 56 mm, hand and head model will be adjusted accordingly in simulation.
- The model for the hand grid is given by the the standard CTIA.
- For measurements two phantom are available depending on the width of the device.

Part I

Analysis

Chapter 2

Theory

2.1 MIMO

2.1.1 Understanding MIMO

MIMO is technique for improving the communication performance by using multiple antennas at the transmitter and at the receiver. By input and output has to be understand the characteristics of the channel that carry the signal not the signal that is applied and received. MIMO can be separated in 3 main groups such as − pre-coding, space multiplexing and diversity coding. Pre-coding is mechanism that allows multiple beams to be released simultaneously in MIMO system. The idea is that to each element of the array is applied specific weighting matrix that allows a specific steerable beam to be created from each element to be produced. In mathematical form:

$$\begin{bmatrix} y^{(0)}(i) \\ y^{(1)}(i) \end{bmatrix} = W(i) \begin{bmatrix} x^{(0)}(i) \\ x^{(1)}(i) \end{bmatrix} \tag{2.1}$$

Where y is the processed signal applied, W is is the weighting matrix and x is the input signal also known as signal layer. This coding allows portion of each signal layer to be transmitted through each antenna. On fig. 2.1 on the facing page is shown the difference of channel with pre-coding and without pre-coding.

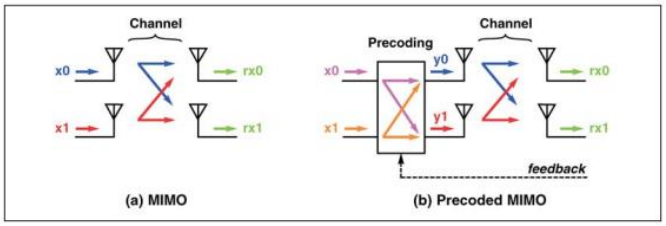

Figure 2.1: *a) MIMO channel without precoding b) MIMO channel with precoding*

Pre-coding requires knowledge for he channel state information CSI. The benefits from this technique are improving the received signal gain and reducing of the multipath fading effect because the signal is emitted from different antennas and is summed up.
Spatial multiplexing is another MIMO technique for which the high bit rate signal is split into low bit rate signal, which are simultaneously transmitted from each antenna in the same frequency channel. If the channel is known at the moment of sending and the signal from different antennas is received with small time delay then the signal are separated like in parallel channels. Spatial multiplexing can be combined with pre-coding for better results. This technique is beneficial mainly for channel with high level of SNR and then the capacity of the system is improved significantly. When spatial multiplexing is used for simultaneous sending of signal to multiple receivers then the technique is known as space division multiple access (SDMA) or multi user MIMO, then is required knowledge of the channel.

Another MIMO technique is diversity coding it is used when there is no knowledge for the channel. The signal is coded with technique called Space Time Coding STC and is transmitted with single beam. STC is a technique that relies on this that the signal is transmitted from all signals and at least one will be delivered trough the physical path to the receiver. There is a diversity of the signal and using multiple transmitting antennas. For this technique there is no beamforming and array gain. In case when there is some knowledge for the channel this technique can be combined with spatial multiplexing.

2.1.2 MIMO in mmobile phones

MIMO antenna system is one of the key technologies of LTE and is also widely used in all modern mobile handsets.It can enhance the channel capacity dramatically compared to the SISO antenna system. However, according to the information theory, the date rate of transmission is

influenced by the signal to noise ratio SNR of the channel and the correlation coefficient between multi elements. The correlation coefficient of the antenna is an important parameter to describe the pattern correlation between the antennas. These parameters can be calculated from the 3-D far-field complex radiation patterns of the antennas, which can be obtained from a numerical method.

Chapter 3

Antenna Investigation

In this chapter an investigation will be presented for two types of antennas suitable for smart phones. At sec. 3.1 will be investigated a PIFA.In 3.2 on page 18 and 3.3 on page 29 two different geometries of printed Monopole antennas are proposed analyzed.In order these antenna to be design and investigated a CST-MS 2013 has been used.

3.1 PIFA Investigation

In this section the characteristics of the PIFA will be investigated, such as reflection coefficient, mutual coupling, radiation and total efficiency, BW and ECC.

3.1.1 Investigation of a Single Element

The geometry of the proposed PIFA is presented in Fig. 3.1 and the idea is adopted from [4, 5]. The longer arm is resonating at $850MHz$ and the shorter at 1700 MHz.

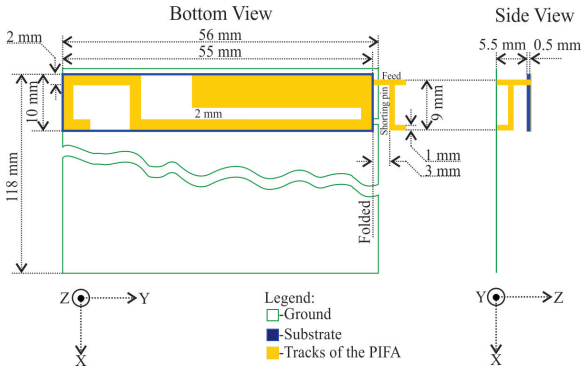

Figure 3.1: *Geometry of the proposed PIFA.*

In Fig. 3.2 is depicted the matching of the antenna with a shorting pin of different length, which represents an inductance in order to cancel out the imaginary part of the impedance of the antenna. As shown in the Fig. 3.2 the antenna without a shorting pin is matched only at 2.6 GHz with a BW of 100 MHz at $S11 = -6\ dB$ recall Sec. 1.4 on page 3.The resonance at 2.6 GHz is the second harmonic of the fundamental frequency of 850 MHz By introducing a shorting pin with different length the antenna is matched better to some frequency than others. By analyzing the Fig 3.2 it is chosen a shorting pin of total length and width of 11x1 mm due to the fact that the two resonances frequencies at $0.850, 1.700$ GHz and the second harmonic of the lowest frequency 2.6 GHz are well matched compared to the other lengths. Moreover, the BWs of operation of the PIFA are show with tag data cursors with the chosen shorting pin(purple color).

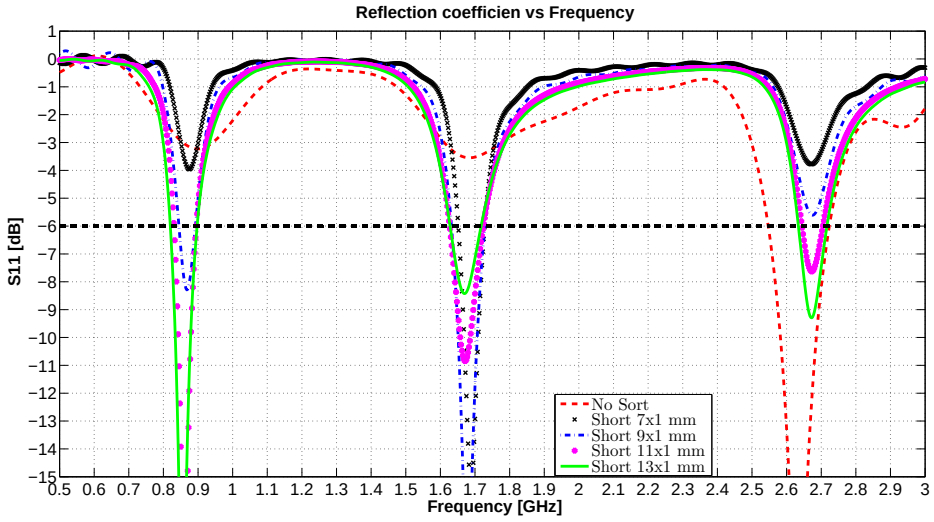

Figure 3.2: *Impedance matching of the PIFA with different total length of the shorting pin.*

The motivation behind this project is recall Sec. 1.1 on page 4, the antenna to be impedance matched to multiple bands under threshold of $S11 = -6\ dB$ and in Fig. 3.2 these bands are not fulfilled.In pursuance of matching the antenna to multiple bands, creating an empty air space slot on the ground , which will produce additional resonance of the antenna and will band together all of the high bands [4, 5].The slot by itself is an aperture antenna, where the in phase voltage gives rise to the radiation from the slot. In Fig. 3.3 on the next page is displayed the effect of the slot to the BW of the antenna. The PIFA achieves a good performance in the high band with the slot of dimensions 1x45 mm and the geometry on this slot is illustrated in Fig. 3.4 on the facing page

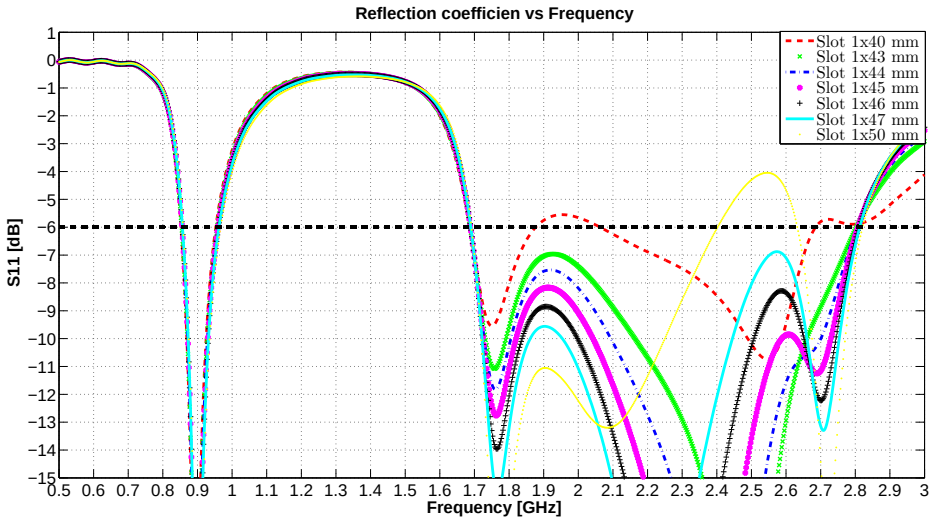

Figure 3.3: *Impedance of the PIFA plus shorting pin and different dimensions of the slot.*

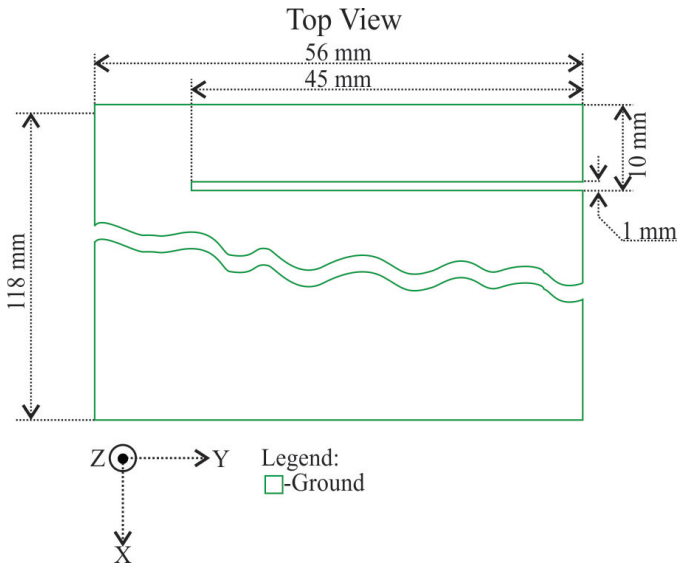

Figure 3.4: *Geometry of the slot on the ground plane.*

To summarize the outcome of adding a shorting pin and a slot on the ground plane is presented in fig. 3.5. The slot with the sorting pin resonate at 2.5 GHz by itself and has approximately BW = 600 MHz at threshold level of $S11 = -6dB$. Introducing the slot, combines three resonance frequencies in the high band and thus all of the required high band are fulfilled, recall once again Tbl. 1.1 on page 4. Moreover, by adding the slot on the ground, the capacitive character of the antenna is decreased, which shift the resonance frequency up wards. Comparing Fig. 3.2 on page 12 and fig. 3.5, the slot boosts the low band by 30 MHz. Nevertheless, from the perspective of the low band the PIFA with short and slot only accomplish the GSM900 band.

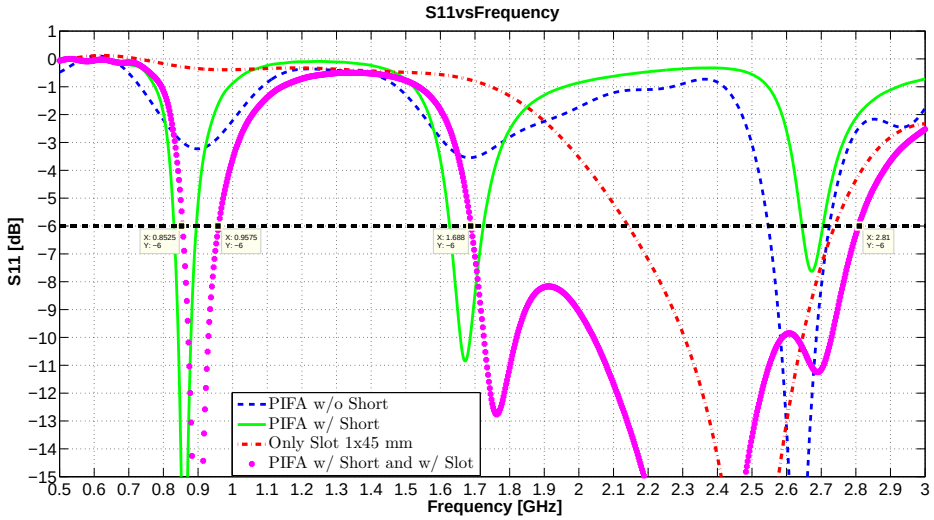

Figure 3.5: *Evaluating the performance of the PIFA by adding a shorting pin and a slot.*

In fig. 3.6 on the next page is displayed the radiation and total efficiency of the antenna. The radiation efficiency is the ratio of the radiated to input power,which includes the conducting and dielectric losses of the antenna. Both in the low and high band, the radiation efficiency(purple curve) is in the range of 82 to 99%. Whereas the total efficiency is a function of the radiation efficiency and the S11 of the single element antenna. Furthermore, where the antenna is impedance matched for example at 0.9, 2.3 and 2.4 GHz the radiation and total efficiency are almost equal. Bear in mind that he total efficiency drops accordingly to the product the radiation efficiency and reflection coefficient in linear or summation in logarithmic scale.

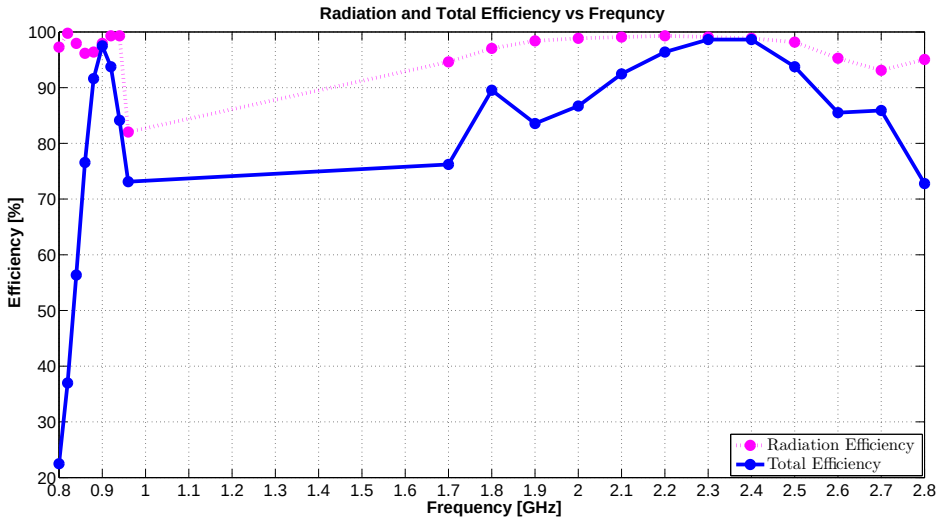

Figure 3.6: *Radiation and Total Efficiency of the PIFA plus Slot.*

3.1.2 Investigation of MIMO

In order to support MIMO an identical element will be placed to the top side of the ground.Two placements have been studied, a rotated and mirror image from the perspective of the primary antenna[6].The geometry of primary and complementary antenna is illustrated in Fig. 3.7.

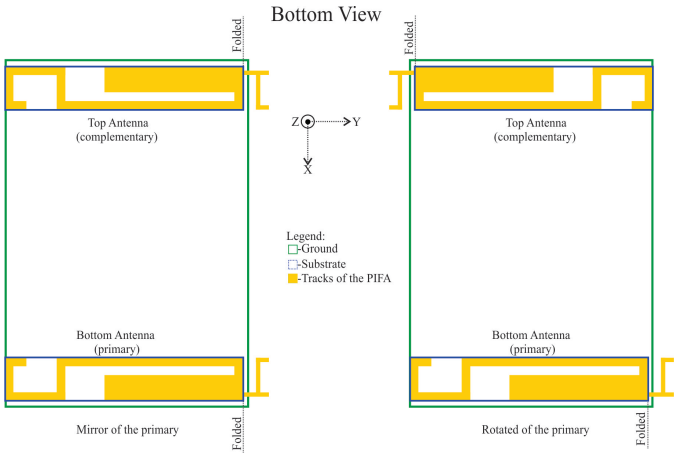

Figure 3.7: *Geometrie of the mirror and rotated MIMO.*

In Fig.3.8 is shown the S-parameters of the mirror BW of the lower band and in opposition the higher bands has been increased slightly compared to the scenario when only one antenna element was present recall Fig. 3.5 on the facing page, due to the coupling between elements.In order to achieve low ECC the coupling between elements has to be as low as possible and in

this project it is set a threshold level $< -8\ dB$.

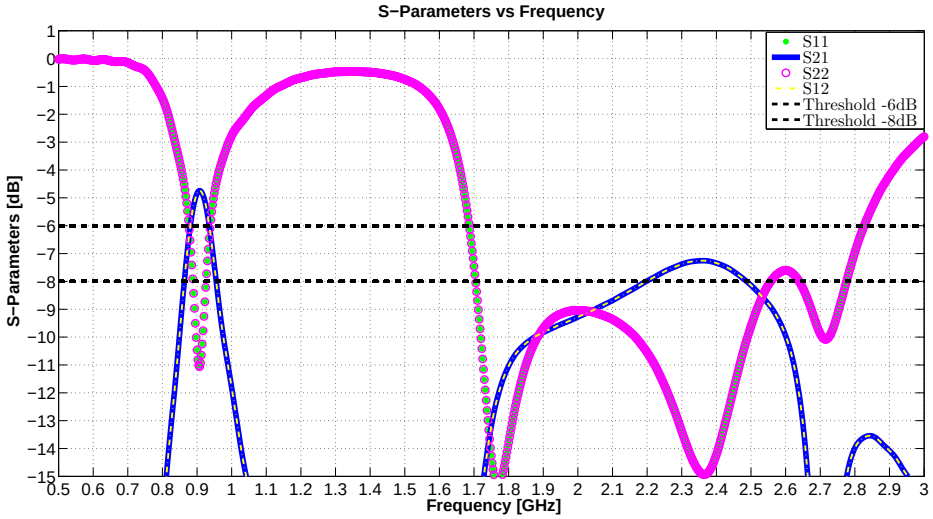

Figure 3.8: *S-parameters of the mirror MIMO.*

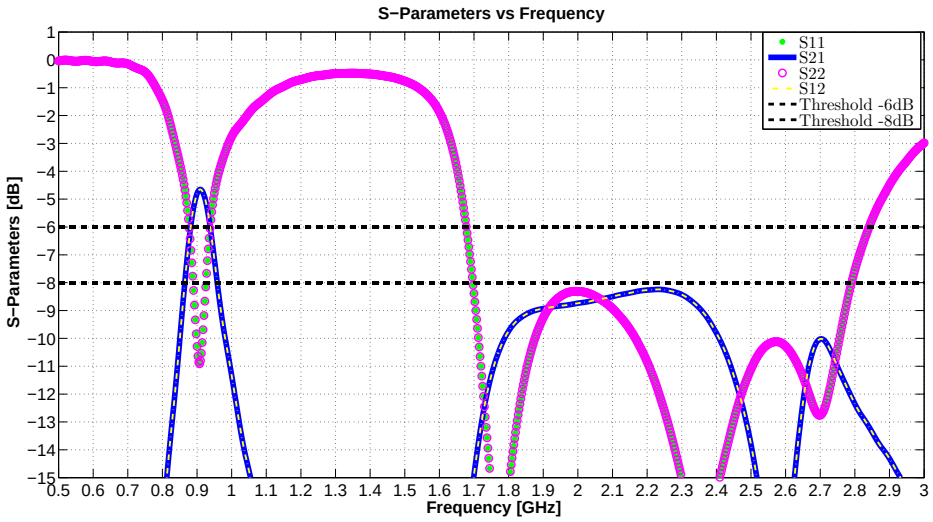

Figure 3.9: *S-parameters of the rotated MIMO.*

In Fig. 3.10 on the next page is depicted the ECC of the mirror and flip complementary antenna. In order MIMO to be implemented recall Sec. 1.4 on page 3 ECC has to be lower than 0.7 for the sake of separating the streams and thus increasing the data rate. Neither of the case displays lower ECC in the GSM 900 band. Although, the results are almost identical in the lower band GSM900, the mirror shows slightly lower ECC. Moreover, the rotated shows lower ECC in the rage of 2.2 to 2.6 GHz. The range of 2.4

to 2.6 GHz is not of interest for the reason that there is a separate WiFi antenna designed in the mobile phones. In the LTE2500 band there is a trade off between mirror and the rotated placement. As a conclusion, the mirror will be manufactured and compared with the simulated results.

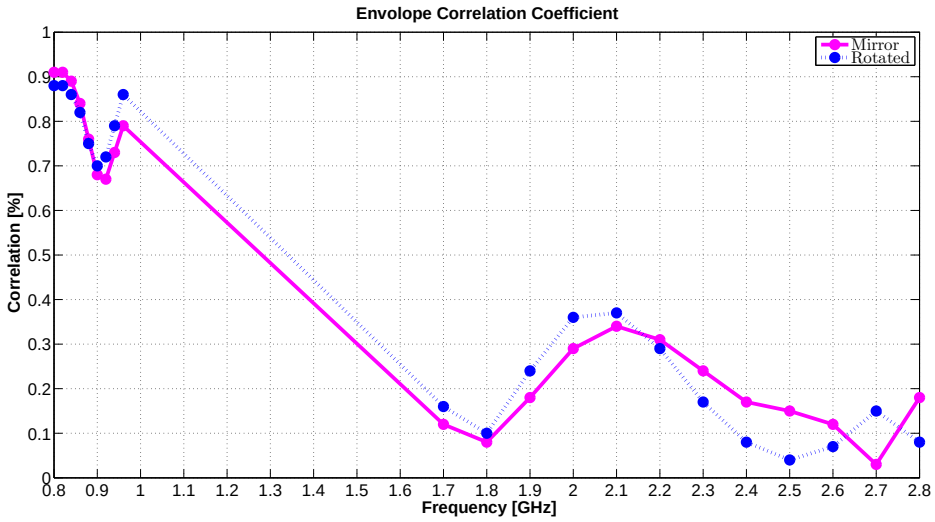

Figure 3.10: *Comparison of the ECC with different antenna placements.*

As a result, embedding the MIMO antenna in a case made out of polymer recall Sec. 1.5 on page 5, the S-parameter were affected. This is illustrated in Fig. 3.11, bear in mind that only the S11 ans S21 are show since the MIMO antenna are symmetrical, which leads to identical S-parameters. Furthermore, analyzing Fig. 3.11, the parameters of the polymer slow down the speed of the electromagnetic wave propagation and as a consequence the matched frequencies of the antenna are shifted down. Hence, the arms of the PIFA were reduced to show similar performance as before.

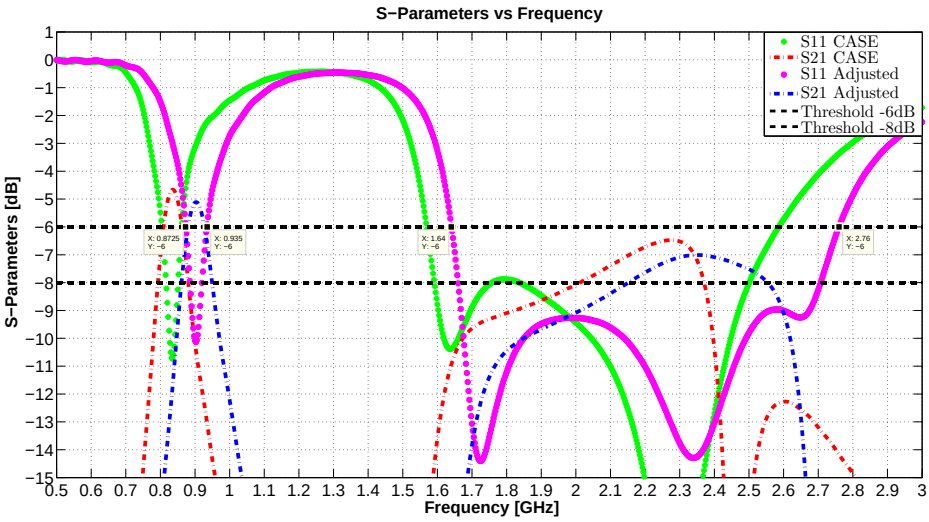

Figure 3.11: *Comparison of the ECC with different antenna placements.*

3.2 Manufactured Monopole Antenna Investigation

In this section is described antenna that is designed to cover all service bands described in Tbl. 1.1 on page 4.The antenna is composed of coupled loop and two arms in order to cover all of them. For the design of the element are used some ideas adopted by paper [8].

3.2.1 Single antenna element and parameter study

First single antenna was designed and simulated in CST. On Fig. 3.12 on the next page is given the geometry of the antenna element with the exact dimensions. The antenna is built on 1 mm tick, 120 mm long, 46mm wide FR-4 substrate ($\varepsilon_r = 4.4$). For the carrier of the antenna is used Arlon ISO 933 ($\varepsilon_r = 4.4$). These materials are selected first of all because they are cheap and easy for manufacturing second the antenna was optimized with them. The overall size of the carrier is 7x11x46mm^3, the geometry of the antenna on the Microwave Printed Circuit Boards (PCB) is shown on Fig. 3.13 on the facing page.On Fig. 3.14 on page 20 is shown the equivalent circuit of the antenna.

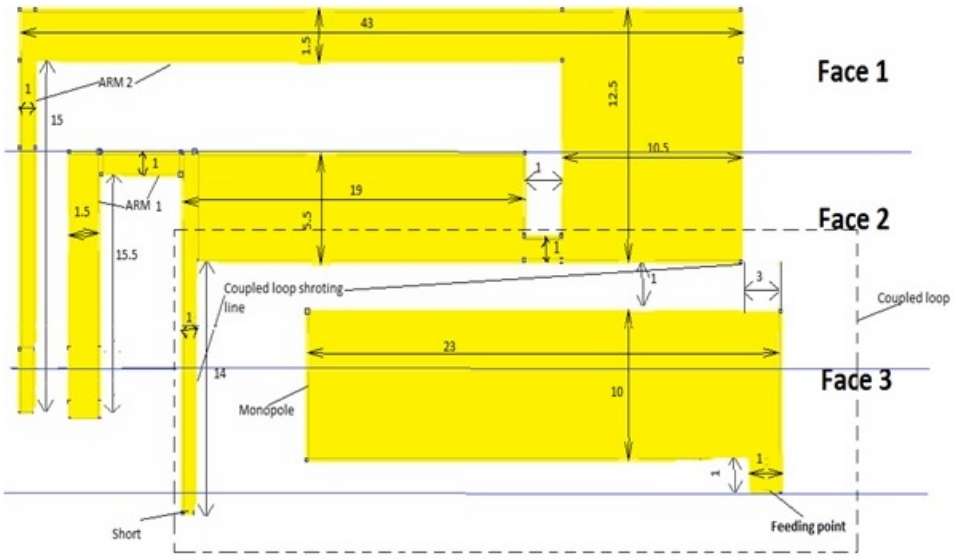

Figure 3.12: *Geometry of the proposed Single element with exact dimensions.*

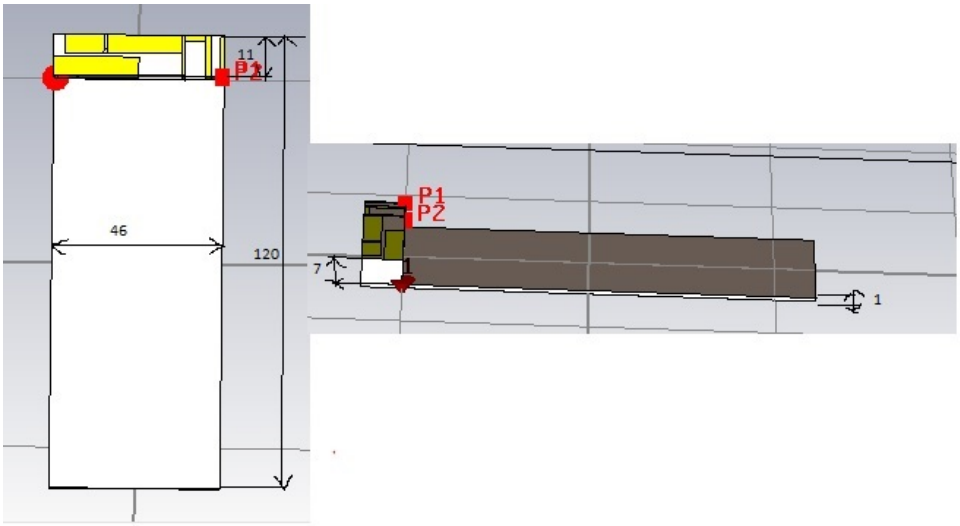

Figure 3.13: *Geometry of the proposed Single element as in CST.*

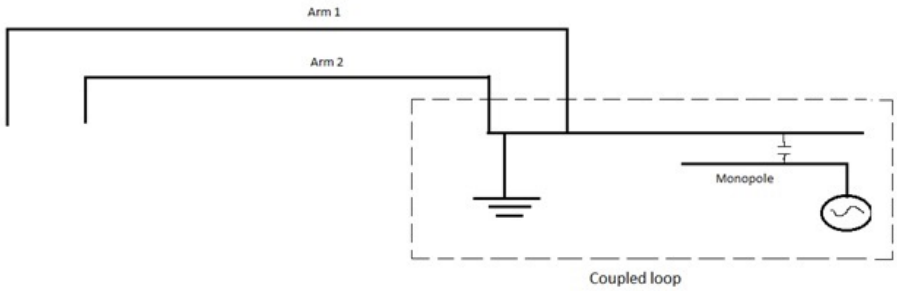

Figure 3.14: *Circuit of the antenna element.*

The antenna consist of two arms (Arm 1 and Arm2) and a coupled loop. The coupled loop is L-shaped monopole and a shorting line. The exact dimensions of the monopole are 10 x 23mm^2 and the length of the shorting line is 44.5 mm, 1 mm wide. On Fig. 3.12 on the preceding page the coupled loop antenna with the shorting line and the monopole is in the dashed line rectangular. The overlapped area between the monopole and the shorting line is 20mm. Arm 2 starts above the shorting line and is 69.5 mm long as shown on Fig. 3.12 on the previous page. The coupled loop and arm 2 resonate at low frequencies – Long Term Evolution (LTE) 700, GSM 850, GSM 900.Arm 1 start above the shorting line and is is 41.5 mm long, as shown on Fig. 3.12 on the preceding page.It is designed in order to resonate in the high frequencies - DCS 1800, PCS 1900 and WCDMA 2100. The monopole is responsible for radiation in the diapason 23000 MHz – 2500 MHz. Also by varying length and width of the monopole is controlled the matching of the antenna.On Fig. 3.15 are shown how which antenna parts cover what bands. The H-filed monitors are shown on Fig. 3.16 on the facing page and 3.17 on the next page where it can be seen which parts radiated in those frequencies.

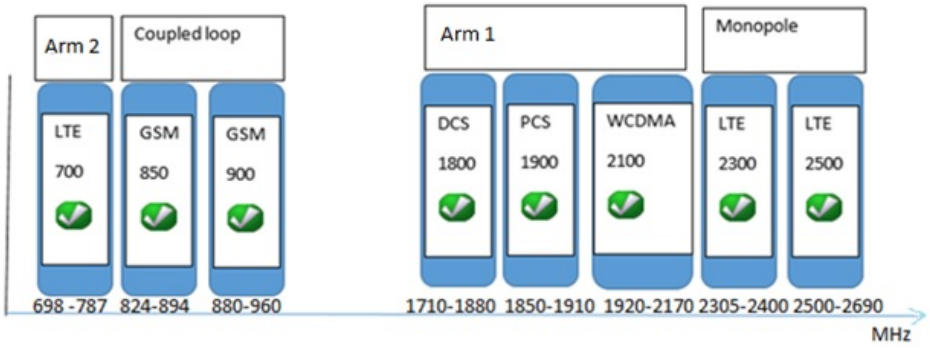

Figure 3.15: *Covered bands by antenna elements.*

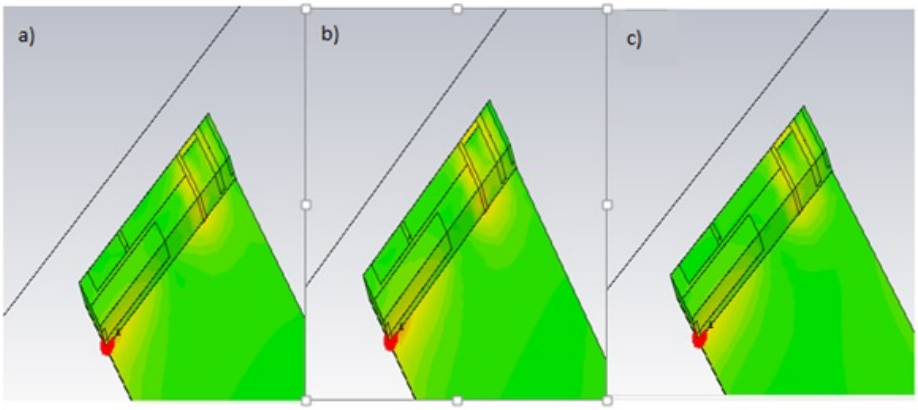

Figure 3.16: *CST H-field monitors a) 2.3 MHz monitor b) 2.5 MHz monitor c) 0.85 MHz monitor d) 0.96 MHz monitor .*

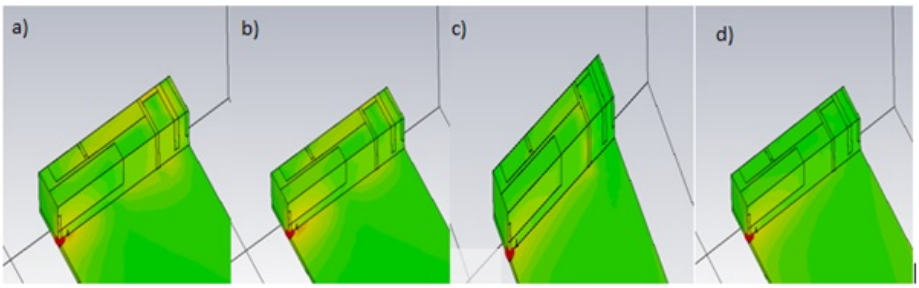

Figure 3.17: *H-field monitors a) 1.710 MHz monitor b) 1.9 MHz monitor c) 2.1 MHz monitor*

On Fig. 3.18 on the following page is shown the S11 parameter of the antenna. The bandwidth (VSWR 3:1) in the low bands is 322 MHz, It covers frequencies from 710 MHz to 1.041 GHz. For the high band the bandwidth is 800 MHz, starting from 1750 to 2550. On Fig. 3.20 on page 23 is presented the efficiency of the antenna. It can be seen that the efficiency is above 48 % for all service bands, which make the antenna element good from manufacturing point of view.

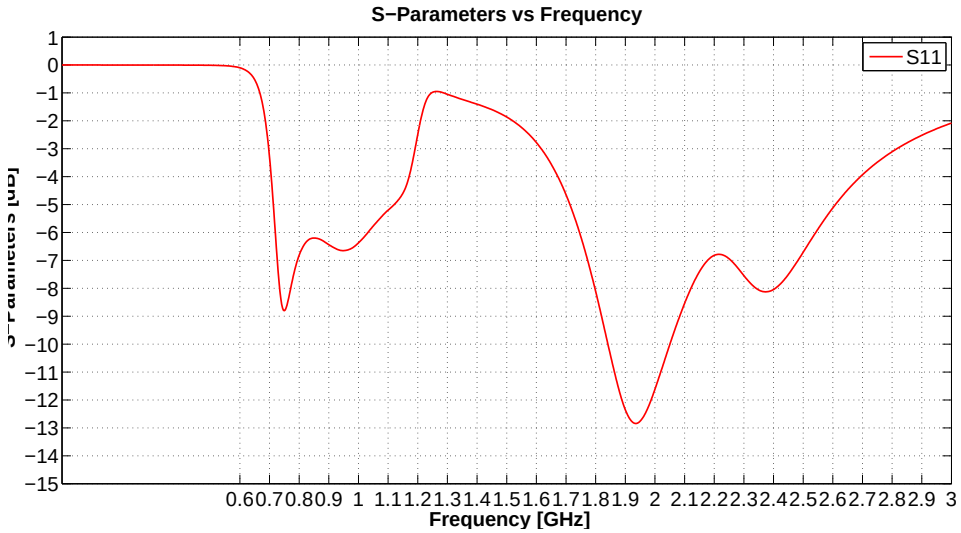

Figure 3.18: *Single element return loss coefficient*

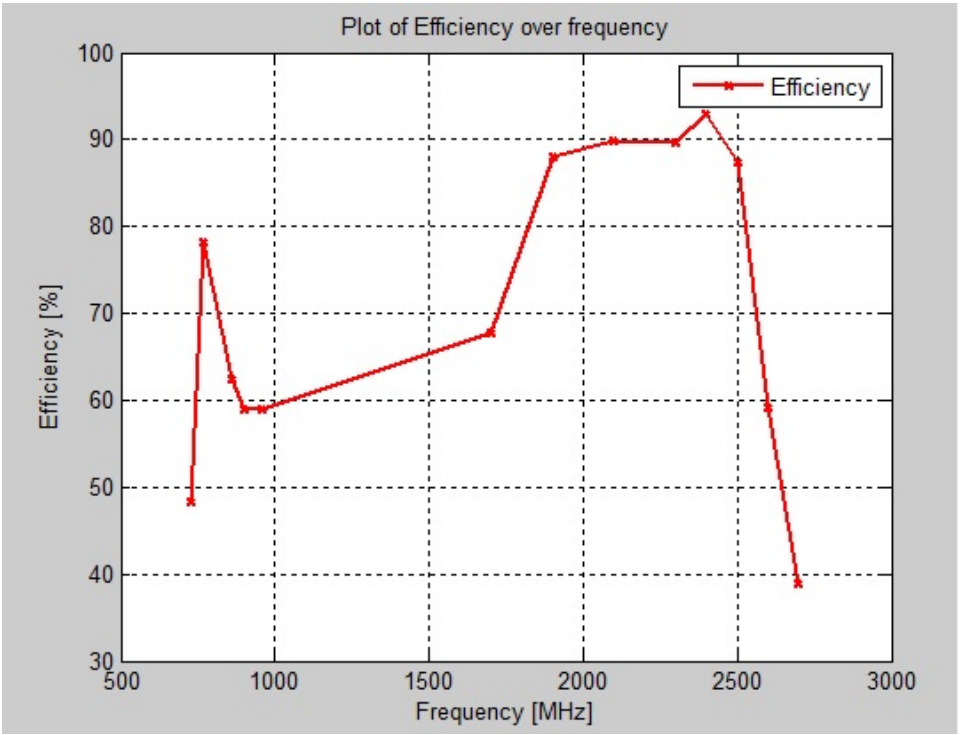

Figure 3.19: *Single elements Total Efficiency*

3.2.2 MIMO antenna element optimal dimensions

From the studied single antenna element are designed two antennas in MIMO configuration. The single element antenna is situated on wider PCB – 1 mm tick, 120 mm long, 64 mm wide, material FR-4 ($\varepsilon_r = 4.4$), also for optimization of the efficiency and s-parameters the dimensions are modified. On Fig. 3.20 are presented the new dimensions of all elements. The overall antenna size is reduced, the carrier is 7x10x45 mm^3. The exact dimensions of the monopole are 8 x 27 mm^2 and the length of the shorting line is 45.5 mm. Arm 1 is with total length of 52 mm and the length of arm 2 is 69mm. 2 MIMO configurations were studied, first one is when the 2 antennas are mirror of each other and on the same opposite sides of the substrate, the second configurations is when the antennas are rotated and on the diagonal sides of the substrate. When the antennas elements are rotated and on the same side, the radiation pattern of the antennas are different and they cover different bandwidths, it's why they can't be used as MIMO. The same is the case when 2 mirrored antennas are put on the diagonals of the substrate.

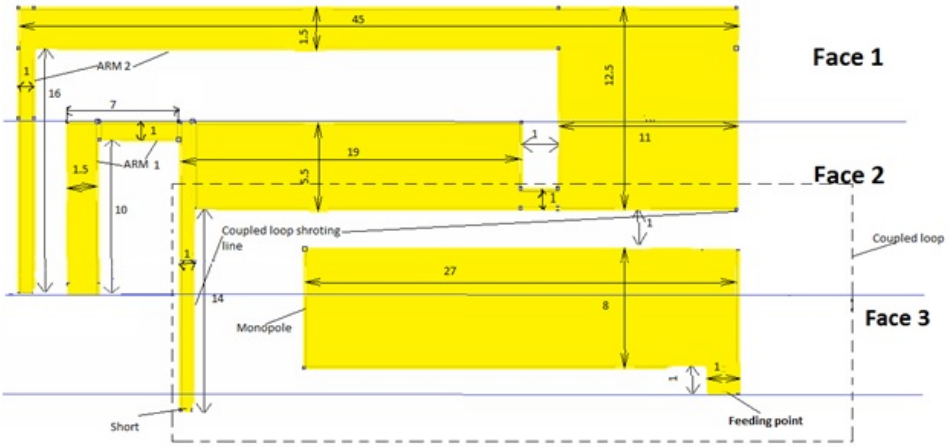

Figure 3.20: *MIMO Single element geometry with dimensions*

3.2.3 MIMO Mirror Same Side

On Fig. 3.21 on the next page is shown the configuration of the 2 antennas. The length of the substrate is 120 mm, each antenna carrier with the antenna on it occupies 10 mm. The ground plane is 100 mm and there is no ground plane under the antennas. In CST are simulated S-parameters of the antennas, the results are presented on Fig. 3.22 on page 25. The bandwidth (VSWR 3:1) for low band is 80 MHz. It covers frequencies from 740 MHz to 820 MHz. For the high band the bandwidth (VSWR 3:1) is 882 MHz, starting from 1678 MHz to 2560 MHz. On Fig. 3.23 on page 25 is shown the efficiency of the antennas, it can be observed that in all bands the

efficiency is above 45%, except in the range 700-730, where it goes to 30% and the after 1650, where the efficiency drops to 35%. Still the achieved efficiency is good from industry point of view. The reasons in the efficiency drop down is the correlation between the 2 antennas. It is plotted on 3.23 on the facing page. In the low frequencies the correlation is above 80% for all frequencies. Low correlation is achieved for the high frequencies.

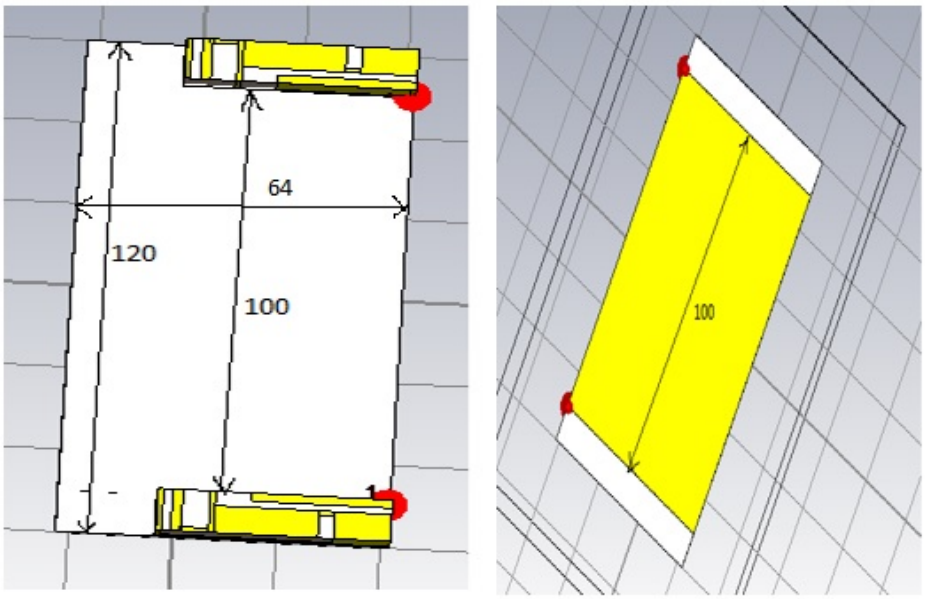

Figure 3.21: *MIMO mirror configuration.*

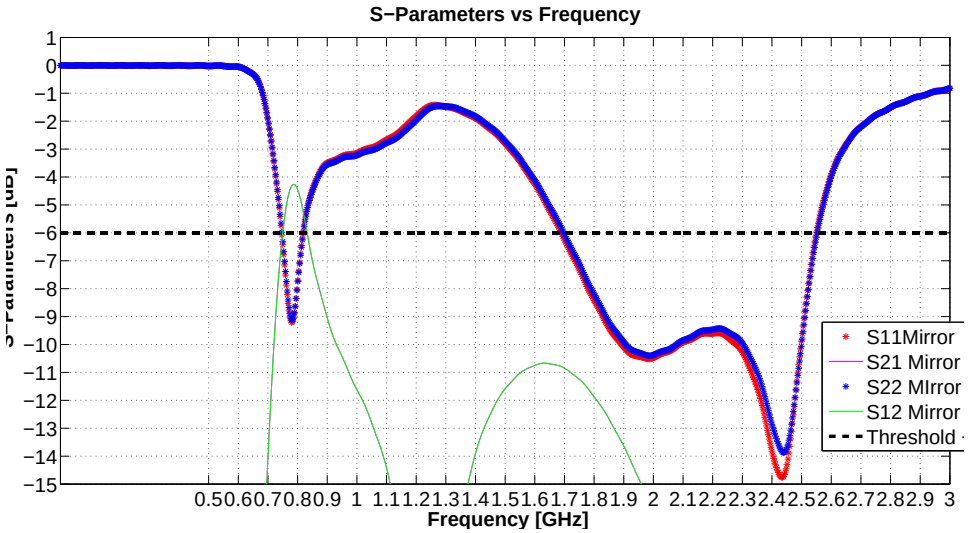

Figure 3.22: *Return loss coefficients of simulated monopole antenna MIMO mirror.*

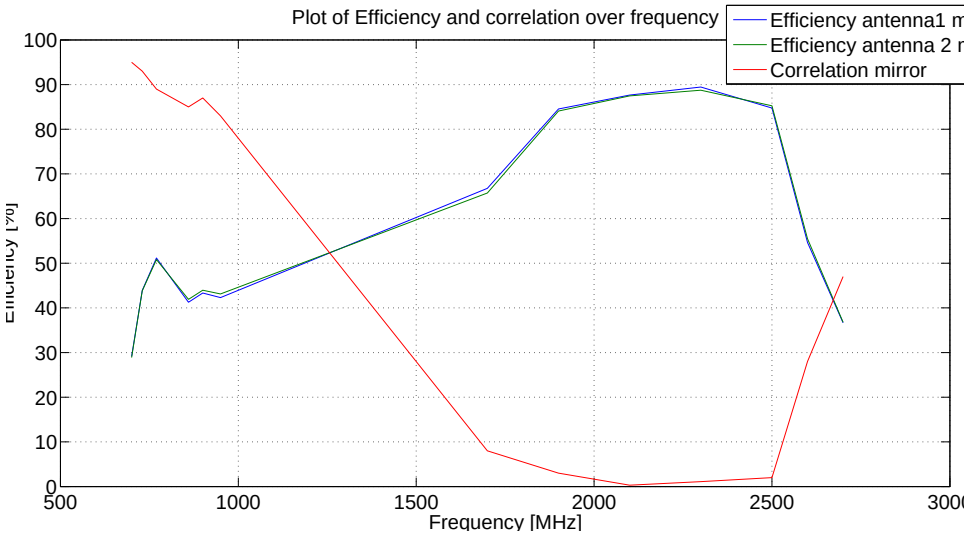

Figure 3.23: *Efficiency and correlation of MIMO mirror*

3.2.4 MIMO rotated diagonal

On Fig. 3.24 is shown the configuration of the 2 antennas. The length of the substrate is 120 mm, width 65 mm, each antenna carrier with the antenna on it occupies 10 mm. The ground plane is 100 mm long, 65 mm wide and there is no ground plane under the antennas. In CST were simulated S-parameters of the antennas, the results are presented on Fig. 3.25 on the facing page. The BW (VSWR 3:1) in the low band is 77 MHz. It covers frequencies from 743 MHz to 820 MHz. For the high band the bandwidth is 882 MHz, starting from 1678 MHz to 2560 MHz. On 3.26 on the next page is shown the efficiency of the antennas, it can be observed that in all bands the efficiency is above 45%, except in the range 700-730, where it goes to 35% and the after 1650, where the efficiency drops to 35%. Still the achieved efficiency is good from industry point of view. The correlation is shown on 3.26 on the facing page. In the low frequencies the correlation is above 80% for all frequencies. Low correlation is achieved for the high frequencies. . In the low frequencies the correlation is above 80% for all frequencies.

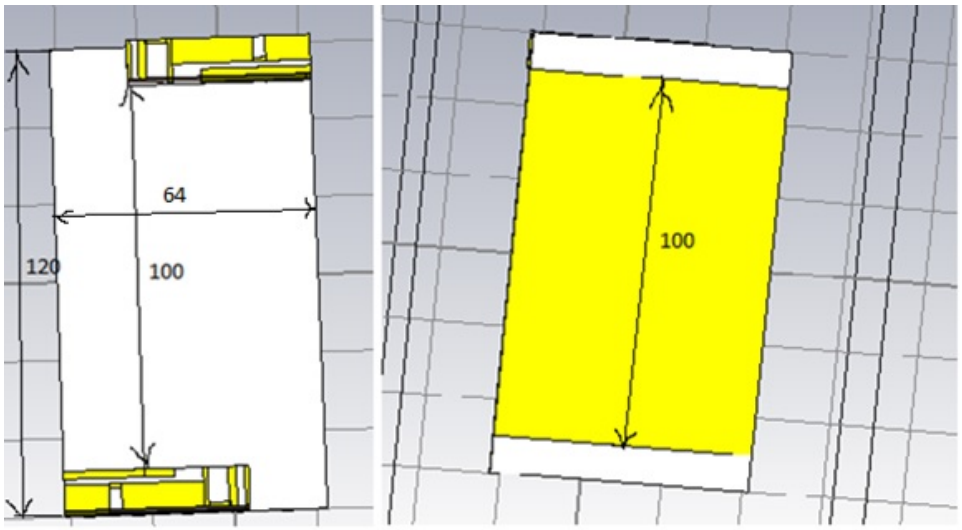

Figure 3.24: *MIMO rotated configuration.*

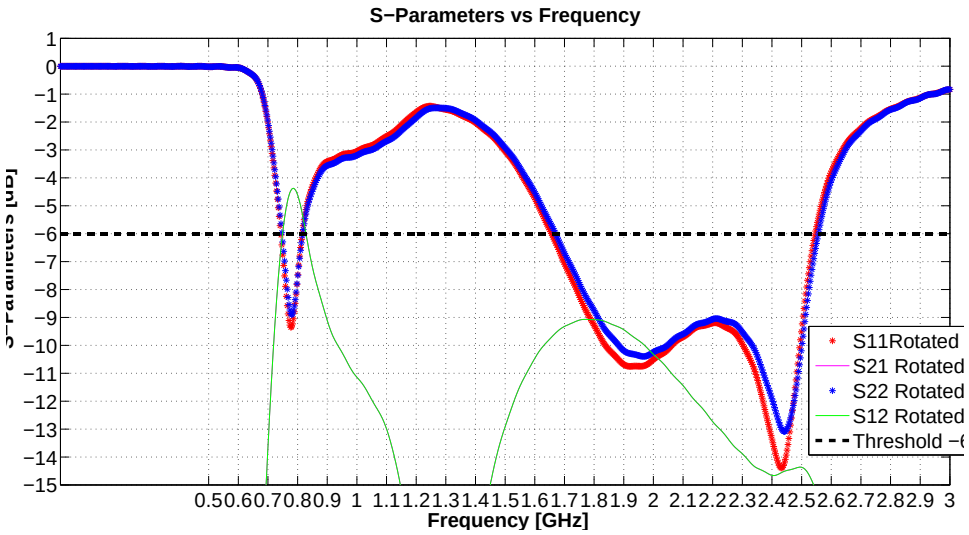

Figure 3.25: *Return loss parameters of MIMO rotated.*

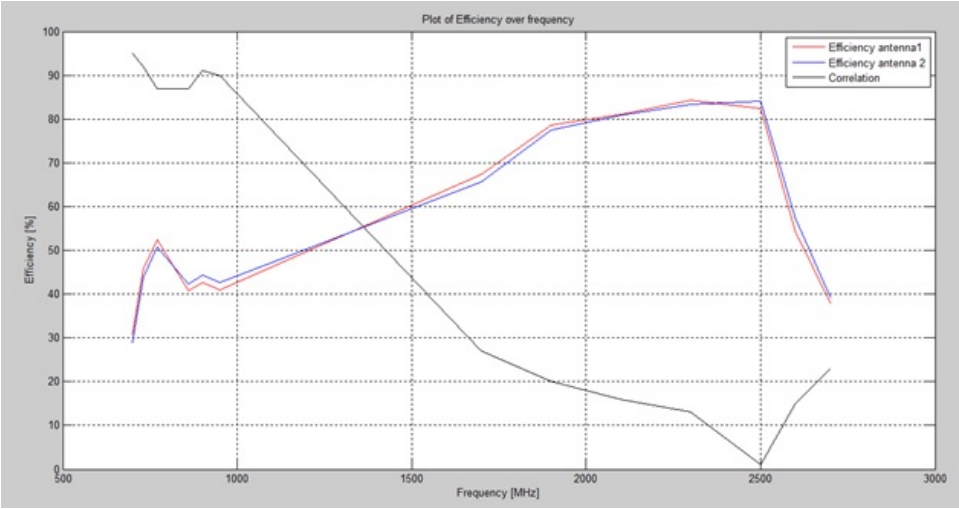

Figure 3.26: *Efficiency and correlation of MIMO rotated*

3.2.5 MIMO configurations comparison

On 3.27 on the next page are shown s-parameters of the 2 MIMO configurations. S12 = s21 of the mirror antenna is lower for the low frequencies, which means that the correlation is lower. The same result is confirmed also by 3.28 on the following page, where is plotted the correlation coefficient. There is a relationship between the correlation and the total efficiency of the antenna as it can be seen on 3.28 on the next page.

Lower correlation between the 2 antennas leads to higher efficiency.Knowing that the correlation is above 80% for the 2 MIMO configurations, every % less correlation meters in assessing MIMO configuration with better performance.That‘s the fact, that in the high frequencies the efficiency is a bit higher for the rotated configuration, is not significant. In summary taking into consideration that the results in the high frequencies are similar or rotated configuration is better but in the low frequencies the mirror configuration shows better results a mock up antenna as per the mirror same side MIMO geometry is built.

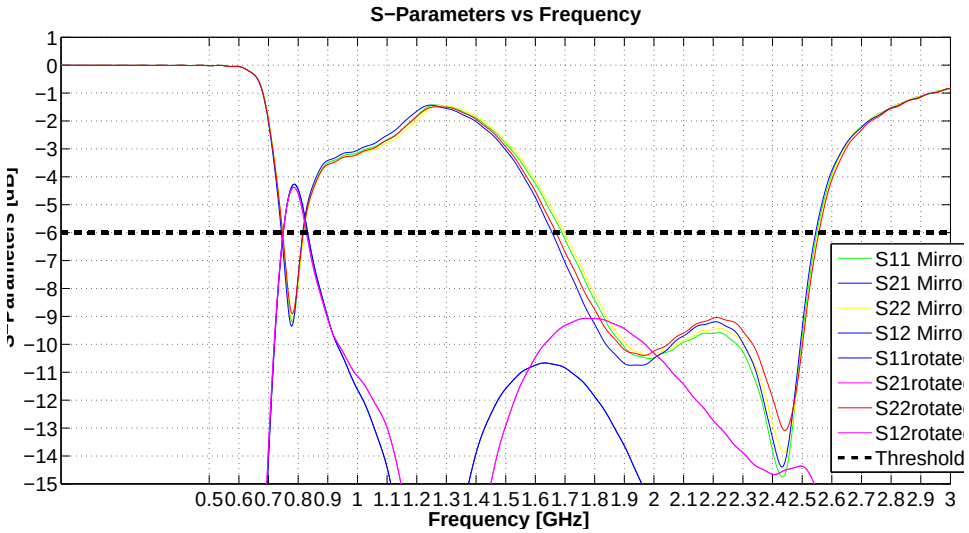

Figure 3.27: *Return loss parameters of MIMO mirror and rotated.*

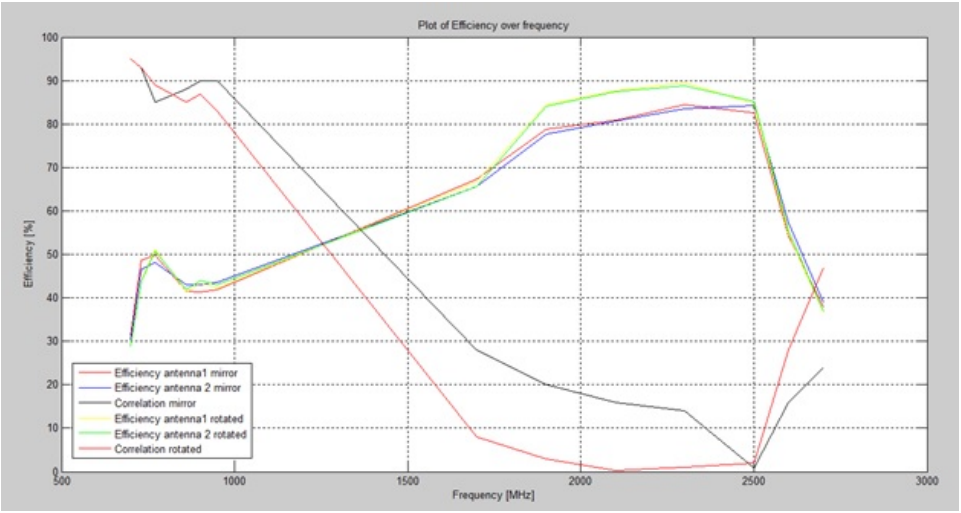

Figure 3.28: *Efficiency and correlation of MIMO mirror and rotated*

3.3 Simulated Monopole antenna

In this subsection is described antenna that covers multiple bands "low band" GSM 850 (824 894 MHz)/GSM 900 (880 960MHz) service band and "High band" for DCS 1800 (1710 1880 MHz)/PCS 1900 (1850 1990 MHz)/WCDMA 2100 (1920 2170 MHz)/LTE 2300 (2305 2400 MHz)/LTE 2500 (2500 2690 MHz) service bands. Some of the ideas for the antenna design are adopted from [9]

3.3.1 Single element study

First single antenna element was designed and simulated in CST. On Fig. 3.30 on the following page is given the geometry of the antenna with the exact dimensions. The antenna is built on 1 mm tick, 120 mm long, 46 mm wide FR-4 substrate $\varepsilon_r = 4.4$. For the carrier of the antenna is used Arlon ISO 933 $\varepsilon_r = 2.33$. These materials are selected because they are cheap and easy for manufacturing also the antenna was optimized with them. The overall size of the carrier is 4x9x45 mm^3. The geometry can be seen on Fig. 3.29 on the next page. One of the antenna arms is folded under the carrier and the other one is on the top of it. The right arm on the top of carrier with the folded part on the bottom is the main radiating element for the lower resonance frequency, and the resonance depends upon the total length of 76 mm , which is approximately $\lambda/4$ of the resonance frequency. Similarly, the left arm is the radiator for the high-frequency band, and the total length is 31 mm equal to $\lambda/4$ of the resonance frequency. The grounded arm is designed to match the impedance of the antenna. The geometry of the antenna as in CST is shown on Fig. 3.31 on page 31. There is no ground

plane under the carrier. On Fig. 3.32 on page 31 is given screen shot with the H-field monitor in the low frequencies, it can be easily observed that the right arm of the monopole is responsible for the radiation. On Fig. 3.33 on page 32are shown the H-field monitors in the high frequencies and it can be seen how with the decrease of the frequency, most of the radiation is moving along on the left arm.

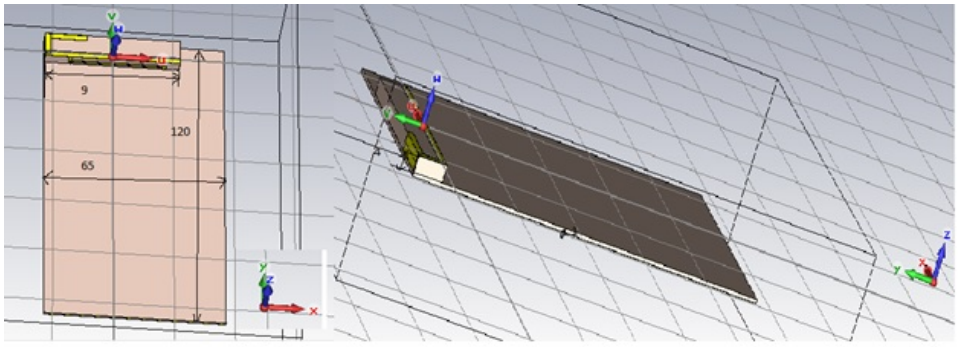

Figure 3.29: *Geometry of the proposed Single element in CST.*

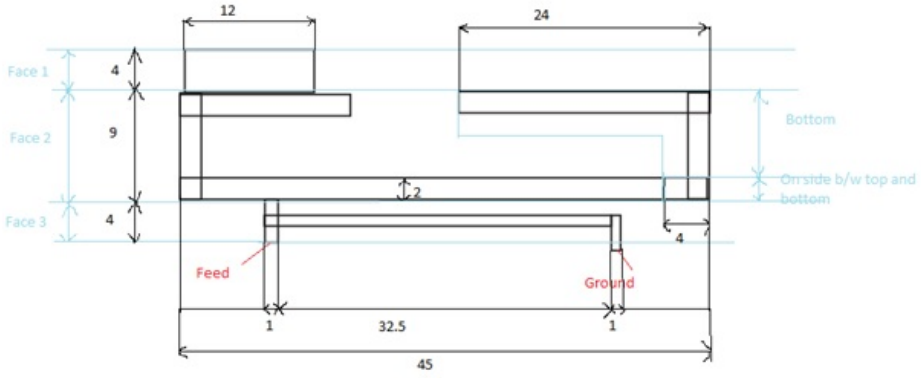

Figure 3.30: *Geometry of the proposed Single element with exact dimensions.*

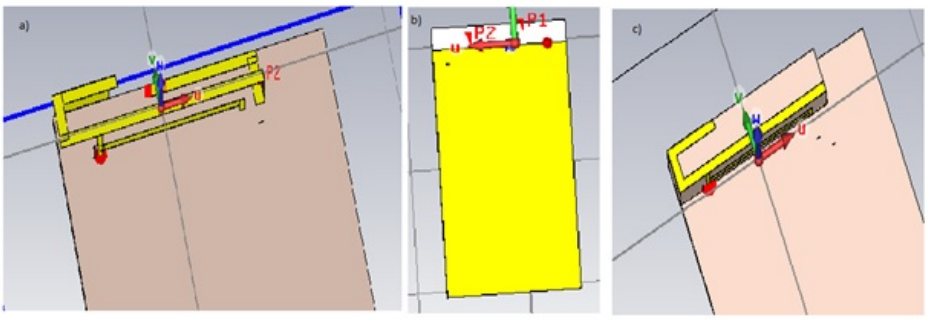

Figure 3.31: *Geometry of the antenna in CST a) Antenna view with hidden carrier b) Ground view c) Antenna view with carrier.*

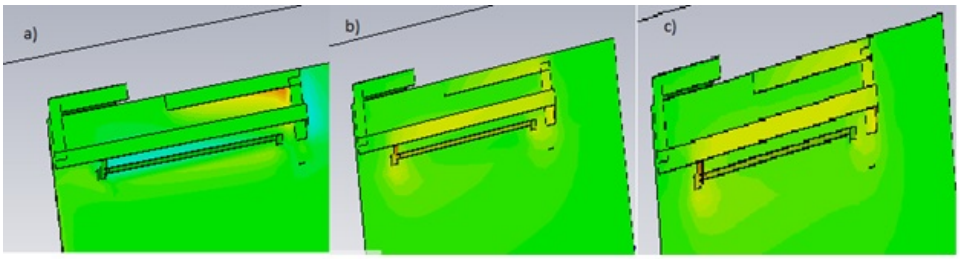

Figure 3.32: *H-Field monitors in the low frequencies a) 850 MHz field monitor b) 900 MHz field monitor c) 960 MHz field monitor.*

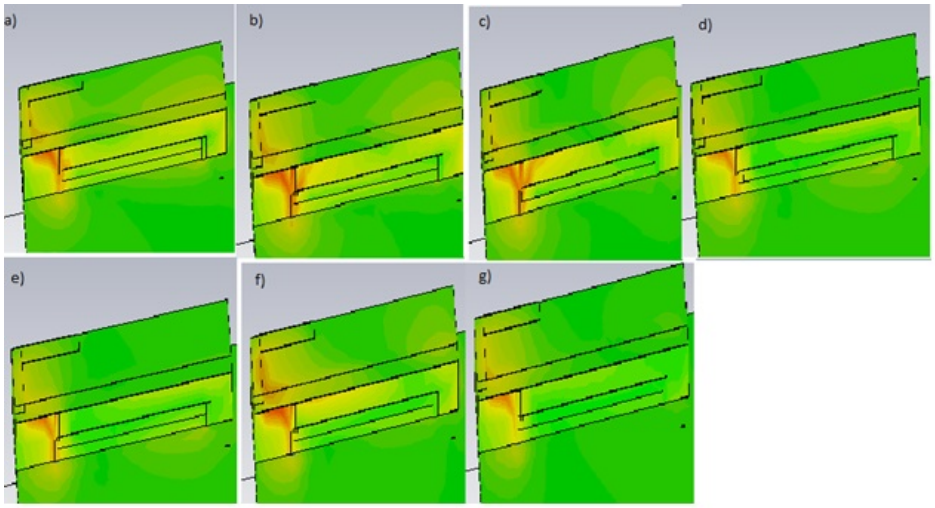

Figure 3.33: *H-Field monitors in the low frequencies a) 1700 MHz field monitor b) 1900 MHz field monitor c) 2100 MHz field monitor d) 2300 MHz field monitor e) 2500 MHz field monitor f) 2600 MHz field monitor g) 2650 MHz field monitor .*

On Fig. 3.35 on the next page is shown the S11 parameter of the antenna. The bandwidth (VSWR 3:1) in the low band is 110 MHz. It covers frequencies from 850 MHz to 960 MHz. For the high band the bandwidth is 1000 MHz, starting from 1700 MHz to 2700 MHz. On Fig. 3.34 on the facing page is presented the efficiency of the antenna. From it can be seen that the efficiency is above 50% for the bands GSM 900 , DCS 1800 ,PCS 1900 ,WCDMA 2100 ,LTE 2300 ,LTE 2500, only for GSM 850 the efficiency drops to 43% but is still sufficient from manufacturing point of view.

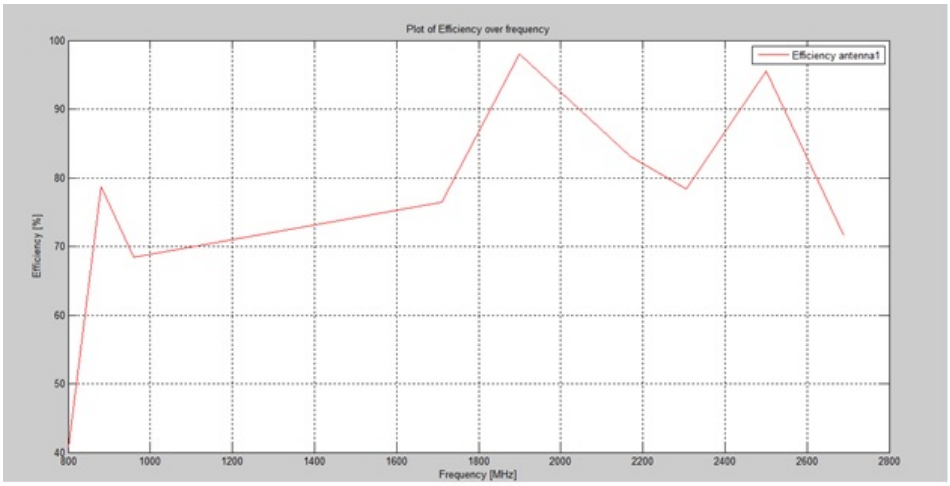

Figure 3.34: *Efficiency of single antenna element.*

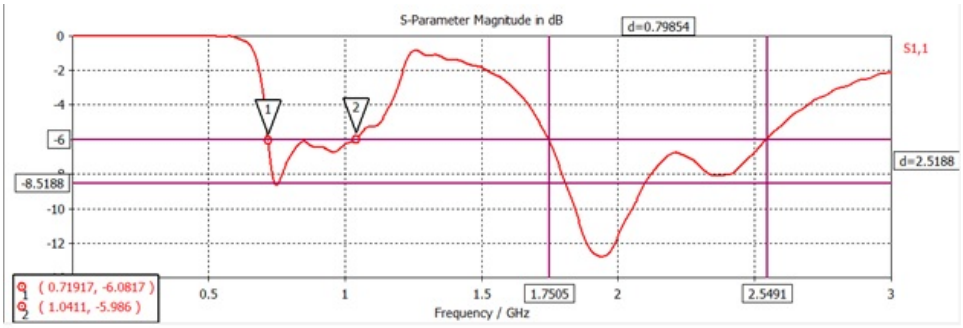

Figure 3.35: *Return loss coefficient of single antenna element .*

3.3.2 MIMO investigation

From the studied single antenna element are designed 2 MIMO configurations. One of the geometries is called MIMO mirror same side and the other is MIMO rotated diagonal. For the mirrored geometry the 2 antennas are positioned in the same corners on 2 opposite sides and the antenna elements are mirrored. For the rotated geometry 2 antennas are on the diagonal corners on the two ends of the substrate in addition the geometry of the element is rotated. In the scenarios with rotated elements on the same side and mirrored elements on the diagonals , the 2 antennas did not cover identical frequency band, due to radiation specifics. Therefore were studied in details the geometries in which s11 and s22 parameters are identical.

MIMO rotated diagonal

On Fig. 3.36 is shown the configuration of the 2 antennas. The length of the substrate is 120 mm, each antenna carrier with the antenna on it occupies 4x9x45 mm^3. The ground plane is 112 mm and there is no ground plane under the antennas. In CST were simulated S-parameters of the antennas, the results are presented on Fig. 3.37 on the facing page. The bandwidth (VSWR 3:1) in the low band is 84 MHz. It covers frequencies from 867 MHz to 944 MHz. For the high band the bandwidth (VSWR 3:1) is 1070 MHz, starting from 1662 MHz to 2732 MHz. On Fig. 3.38 on the next page is shown the efficiency of the antennas, it can be observed that in all bands the efficiency is above 40%. Still the achieved efficiency is good from industry point of view. One of the reasons for the efficiency decrease is the correlation between the 2 antennas. The correlation is shown on on same Fig. 3.38 on the facing page. In the low frequencies the correlation is above 80% for all frequencies. Low correlation is achieved for the high frequencies.

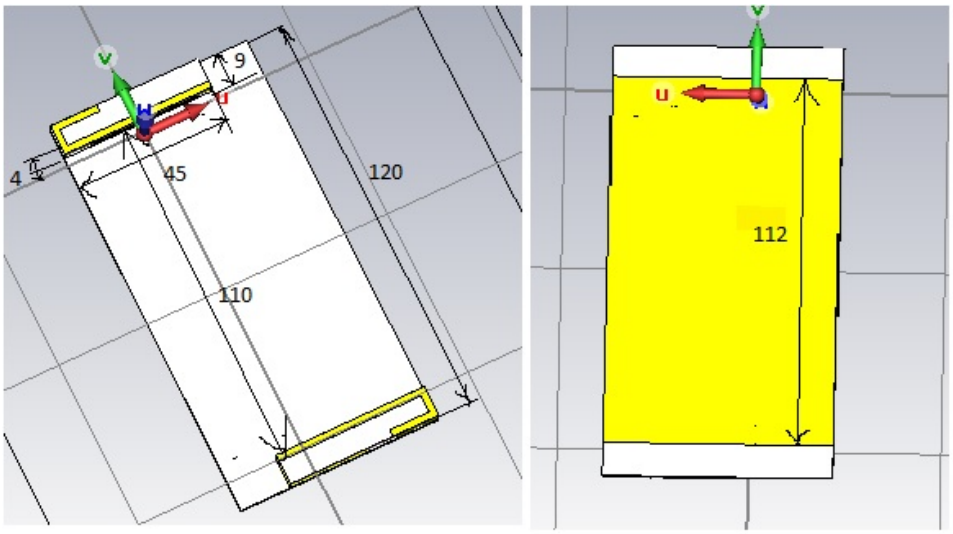

Figure 3.36: *Geometry of MIMO rotated as in CST.*

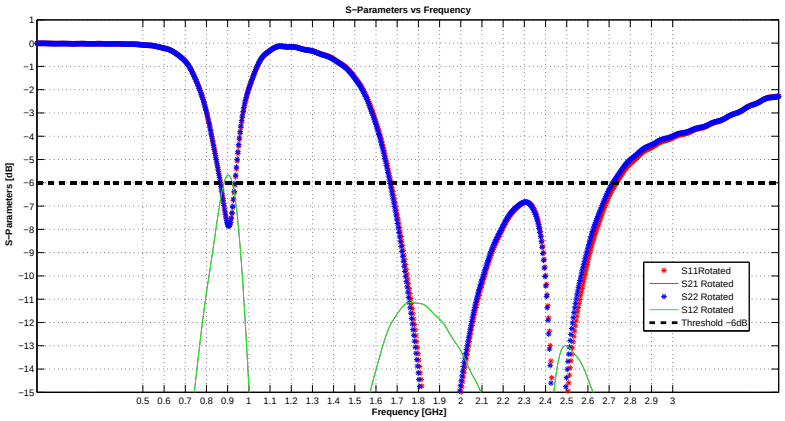

Figure 3.37: *Return loss coefficient of MIMO rotated.*

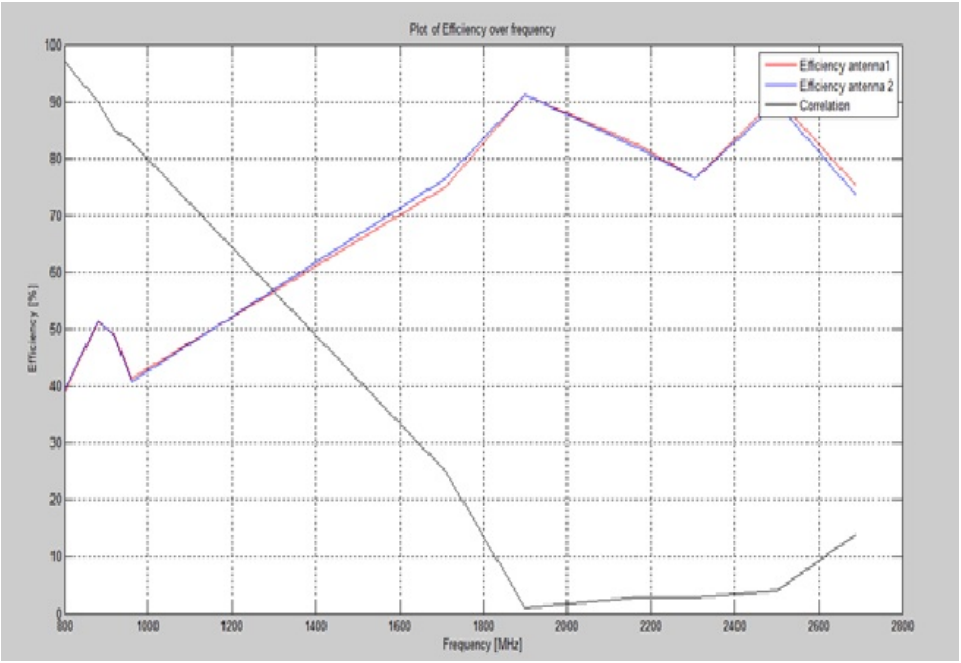

Figure 3.38: *Efficiency and correlation of MIMO rotated.*

MIMO mirror same side

On Fig. 3.39 is shown the configuration of the 2 antennas. The length of the substrate is 120 mm, each antenna carrier with the antenna on it occupies 4x9x45 mm^3. The ground plane is 112 mm and there is no ground plane under the antennas. In CST were simulated S-parameters of the antennas, the results are presented on Fig. 3.40 on the facing page. The bandwidth (VSWR 3:1) in the low band is 84 MHz. It covers frequencies from 867 MHz to 944 MHz. For the high band the bandwidth is 1033 MHz, starting from 1676 MHz to 2710 MHz. On Fig. 3.41 on the next page is shown the efficiency of the antennas, it can be observed that in all bands the efficiency is above 40%. Still the achieved efficiency is good from industry point of view. One of the reasons for the efficiency decrease in comparison with the single element is the correlation between the 2 antennas. The correlation is shown on Fig. 3.41 on the facing page. In the low frequencies the correlation is above 80% for all frequencies. Low correlation is achieved for the high frequencies.

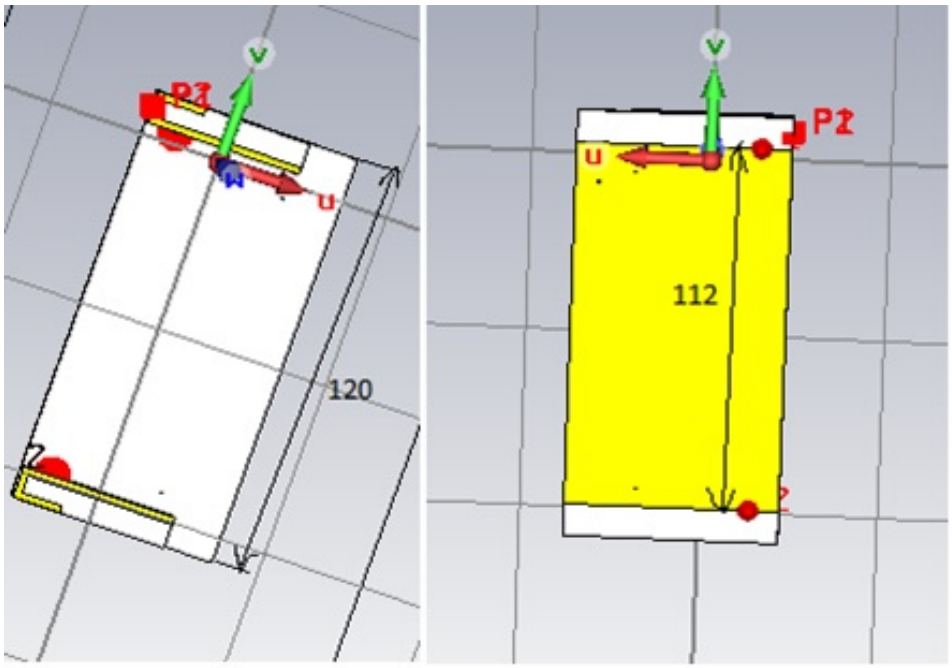

Figure 3.39: *Geometry of MIMO mirrored as in CST.*

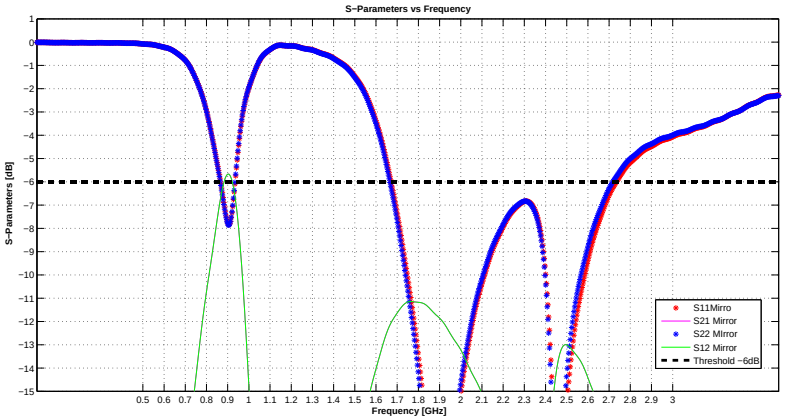

Figure 3.40: *Return loss coefficient of MIMO mirrored.*

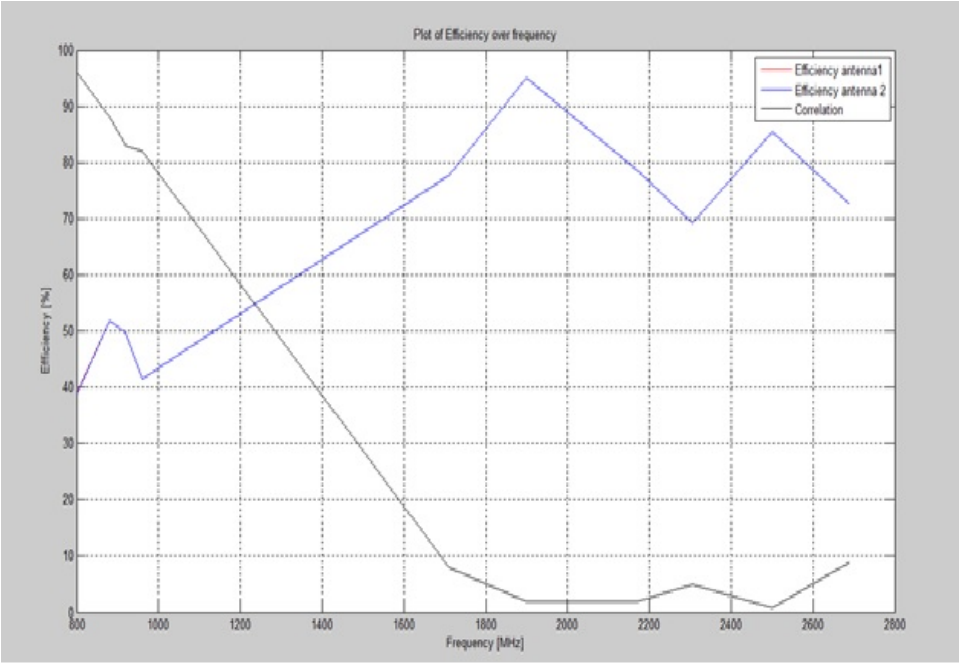

Figure 3.41: *Efficiency and correlation of MIMO mirrored .*

3.3.3 MIMO comparison

On Fig. 3.42 are presented s parameters of the MIMO configurations from it can be seen that they cover the same BW range in low frequencies, rotated configuration covers a bit wider BW in the high frequencies.$S12 = S21$ parameters shows the correlation in the 2 MIMO geometries. When the antennas are on the same side mirrored to each other it can be seen that the correlation is lower in low frequency band than the other scenario. On Fig. 3.43 on the facing page is given efficiency and correlation for the 2 MIMO cases, the lower correlation is confirmed from the data in CST. In addition efficiency in low frequency is higher for this the antennas on the same side. This antenna configuration has better performance in terms of lower correlation and higher efficiency which makes it more promising from manufacturing point of view.

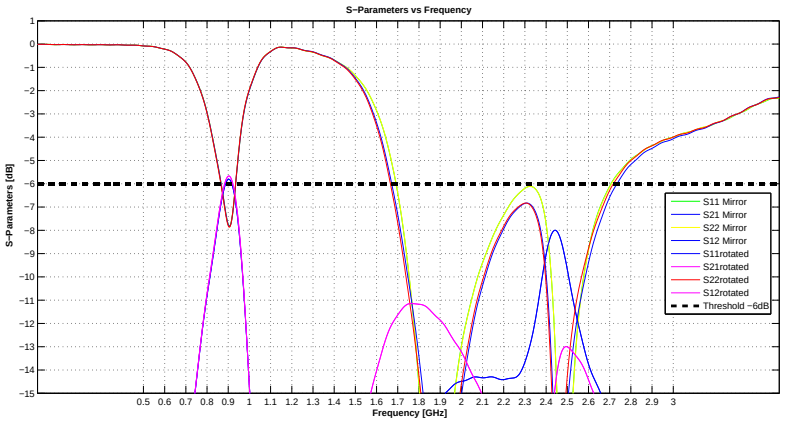

Figure 3.42: *Return loss coefficients of 2 MIMO configurations .*

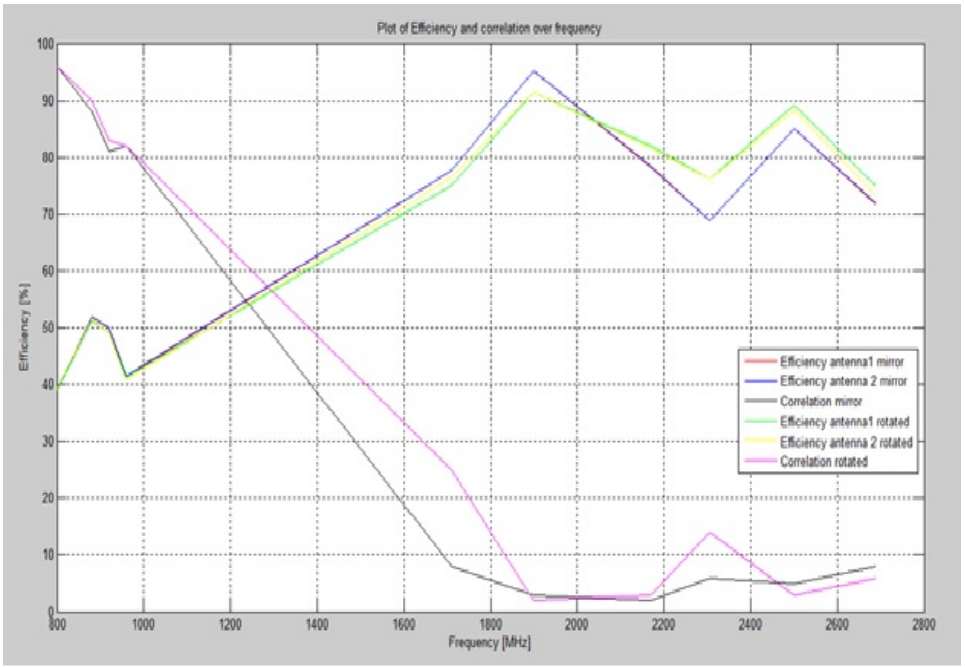

Figure 3.43: *Efficiency and correlation of MIMO configurations.*

Chapter 4

Cable effect investigation

This capter aims to deal with the mismatches and uncertainties in the measurements due to cables.
Different positions of the antenna feeding cable are simulated for single antenna element of the manufactured monopole antenna as described in 3.2.1 on page 18 . Simulations with infinity long cable are done in order to avoid dependence of cable length and to assure that observed results are due to the cable effects. Two sets of simulation were done. One is with infinitely long cable going out of the ground, simulated are several cable positions in the corresponding point of interest as shown on Fig. 4.1 on the facing page. Second set of simulation is with cable that is bent out of the ground as shown on Fig. 4.2 on the next page. The aim of the 2 sets of simulation is to investigate how the cable effects bring uncertainty and mismatch losses in the return loss coefficients.

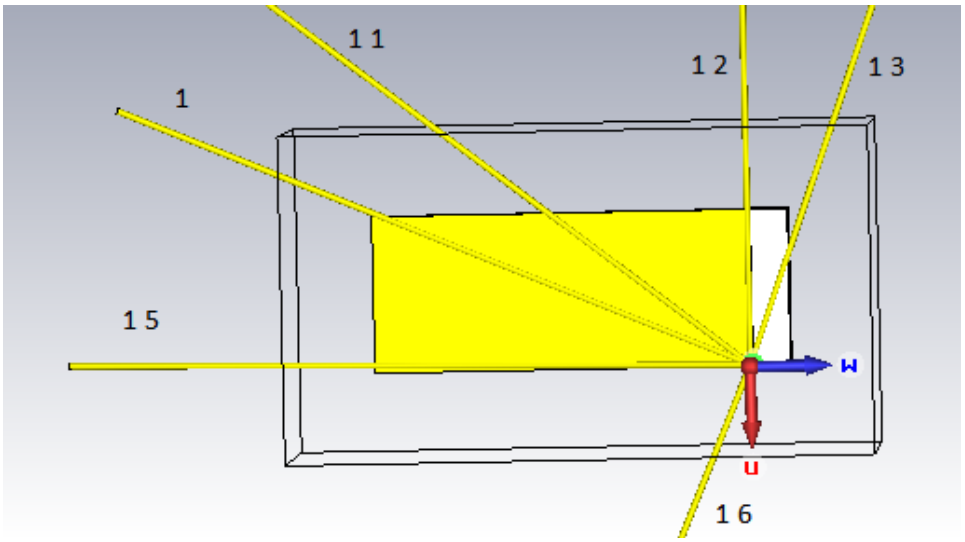

Figure 4.1: *Different position of the cable on the ground for set of simulations 1.*

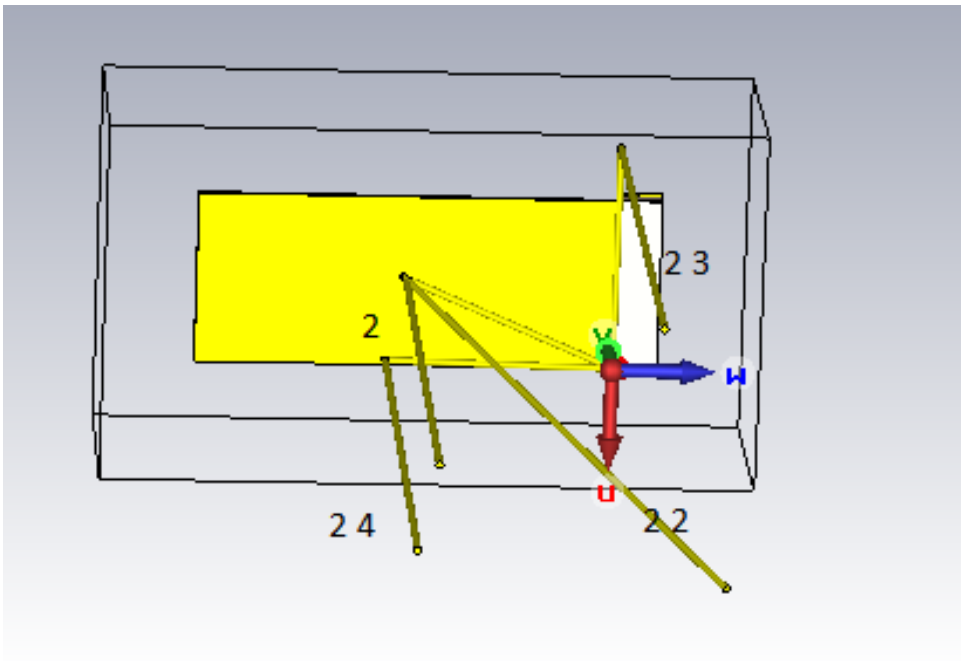

Figure 4.2: *Different position of the cable on the ground for set of simulations 2.*

All simulated return loss coefficients for set of simulation 1 as shown on Fig. 4.3 are presented on Fig. 4.1 on the previous page. It is observed that when the cable is under the antenna element, where there is no ground, this seriously affects s11 parameters of the antenna. Resonant frequencies are shifted to left, this effect is due to the resonating model of the monopole which should have no ground under the antenna‘s element. Another point of interest with big ripples in the result and a lot of mismatching is when the cable attached to the ground at one point under the feeding point and most of it is out of the ground, position 1 6. In the low frequencies s11 parameter of the antenna show that it is resonant only in the range (VSWR 3:1) from 710 MHz to 795 MHz. For this position of the cable a lot of ripples are observed in s11 parameter plot.

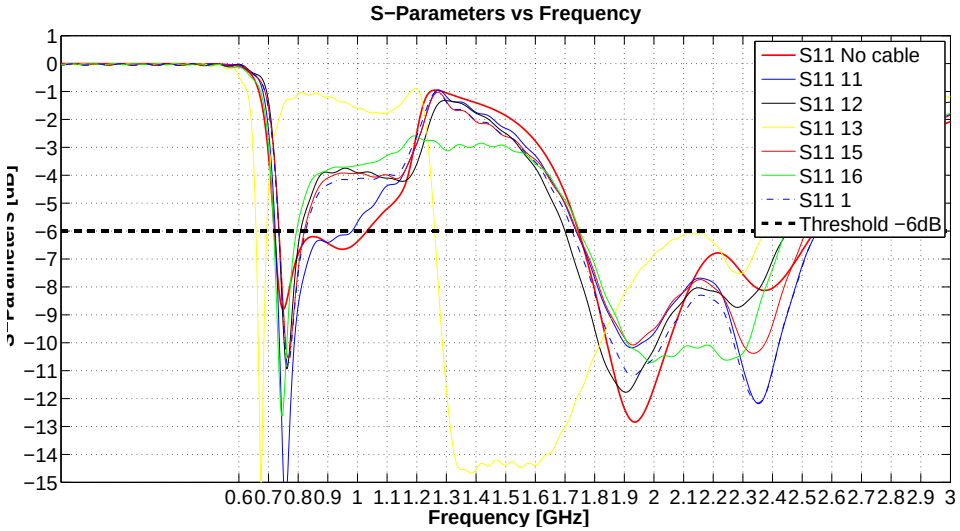

Figure 4.3: *Return loss coefficients for set of simulations 1.*

When the cable is lying on edges as in positions 1.2 and 1.5 on Fig. 4.3 it can be seen that s11 parameters are with uncertainties and mismatches in the low frequencies. Best results are shown when the cable is close to the the middle of the ground, touching one of the edges as in position 1 1. on Fig. 4.4 on the next page are shown H-field monitors and analyzing them it can be concluded that at the position of the cable 1 1 the cable and the ground are less excited. In general it is observed that around the edges the current is higher and it has minimum in the middle of the ground.

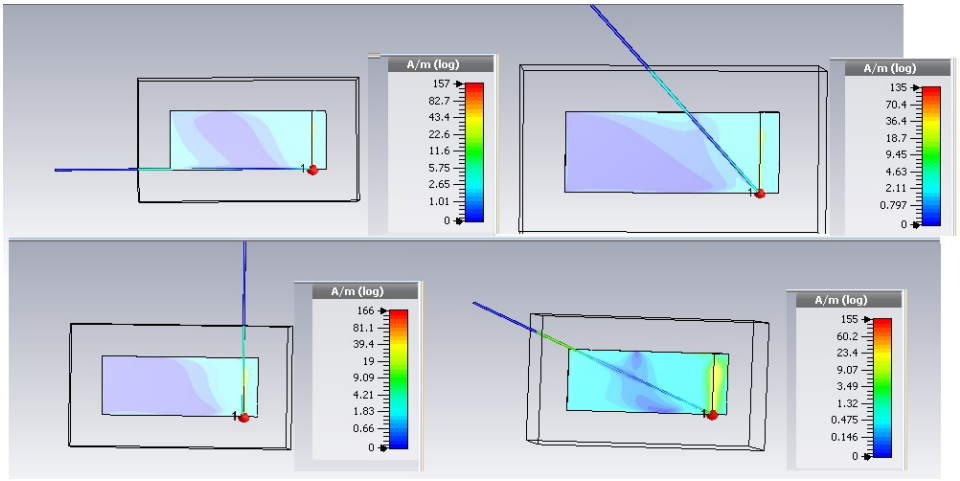

Figure 4.4: *Return loss coefficients for set of simulations 1.*

Knowing that magnetic field has it's minimum in the middle of the ground, set 2 of simulations as shown Fig. 4.2 on page 41 was done. The cable was bent in the center of the ground and pointed perpendicularly towards infinity.Return loss coefficients for all simulation are shown on Fig. 4.3 on the preceding page. Best results are observed for the two positions where the cable is bent in the center of the ground. On Fig. 4.6 on the following page are shown current distribution from the CST H-field monitors, it can be seen that ground and cable are more excited when they are on the edges and out of the ground.

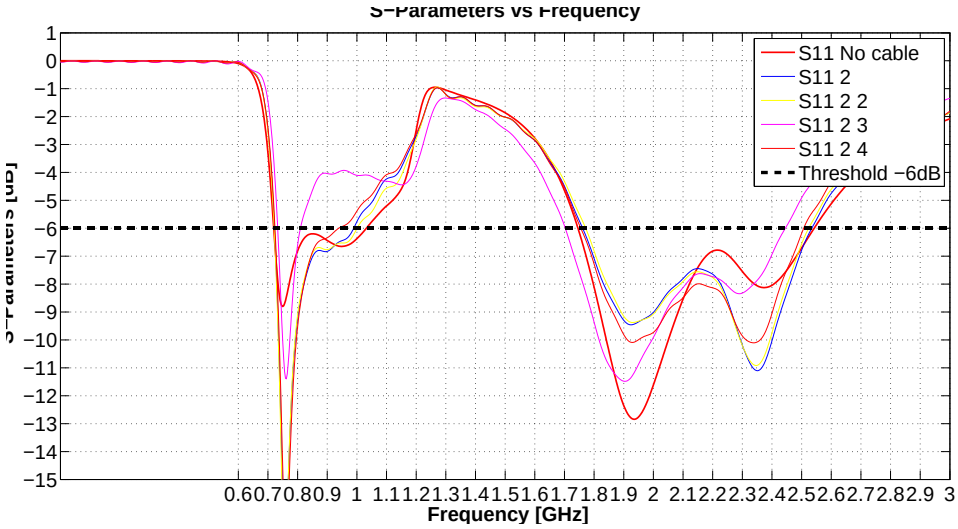

Figure 4.5: *Return loss coefficients for set of simulations 1.*

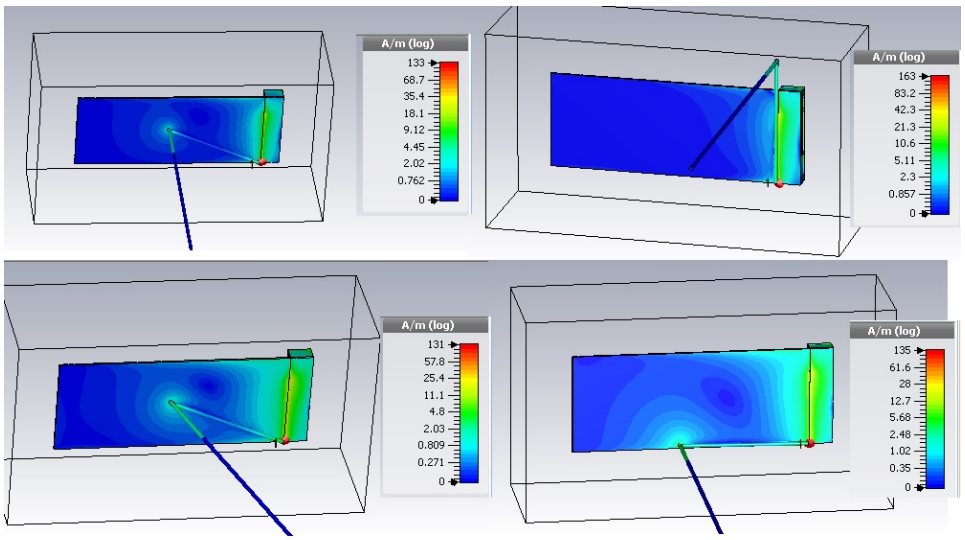

Figure 4.6: *Return loss coefficients for set of simulations 1.*

From all simulations of the cable positions it can be concluded that the best position for the cable is where the magnetic field is minimum. From manufacturing point of view when the the feeding cables are soldered to the antenna ground this has to be taken into account. For the studied single element it‘s best those cables to be soldered from the center to the feed and bent perpendicularly. As it can be seen from the simulation when the antenna elements are measured the cables from the VNA will affect the measurements. That‘s why for eliminating the effect of the cables chokes must be used. They are described in the next chapter.

Chapter 5

Balun Investigation

5.1 Investigation of the Bazuka Balun for different position from the antenna.

In order to investigate the balun, a dipole antenna as a reference has be used due to the fact that its parameters are well known.In Fig. 5.1 is shown the scenario under test in CST-MS.

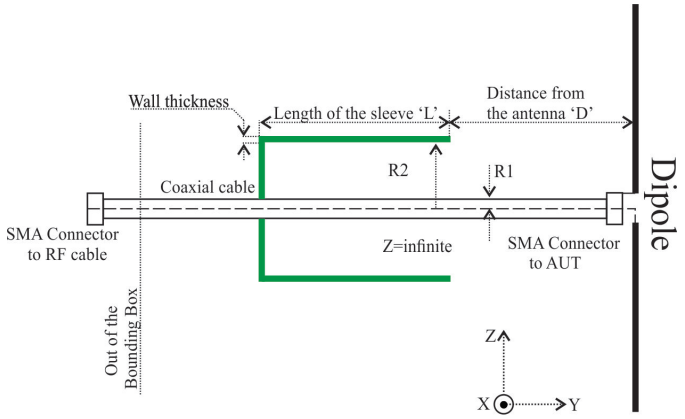

Figure 5.1: *Scenario under investigation for the balun.*

In Fig. 5.2 is displayed the effect on the impedance of the dipole without and with a balun at different positions from the dipole. In addition in Tbl. 5.1 is presented description on the legend displayed in Fig. 5.2.As a result, in Fig. 5.2 it is evident that moving the balun further away from the dipole, a parasitic arm to the dipole is created, which produce superious radiation and the reference dipole and the dipole with balun are not in perfect agreement. Shorter parasitic arm will produce resonance at higher frequency as $\lambda/20$ at 3 GHz; controversially longer parasitic arm will produce resonance at low frequency as $\lambda/2$ at 1.8 GHZ. Furthermore, the curve with

distance $\lambda/20$ shows good agreement with the reference dipole and thus it is chosen as the best position in this scenario.

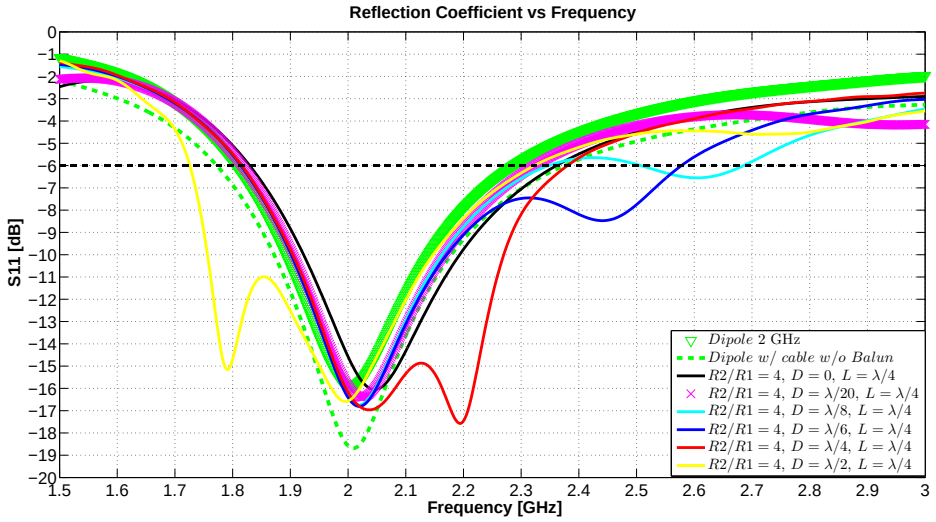

Figure 5.2: *Comparison of dipole impedance w/ and w/o Balun.*

Indication	Description
$R2/R1$	Ratio of the inner radius of the balun and the RF coaxial cable.
D	Position away from the dipole.
L	Length of the balun.

Table 5.1: *Description of the legend.*

In Fig. 5.3 it is depicted the comparison of the reference dipole directivity in dBi at 2 GHz with and without the balun at $\phi = 90°$ and cut in elevation plane.In addition the balun is placed at spherical coordinates of $\theta = 270°$ and aligned with $\phi = 90°$ and $\phi = 270°$.Two are the worst cases, which produce degradation in the radiation pattern. First, when the dipole is attached an infinite RF cable, notice the range from $\theta = 180°$ to $\theta = 360°$, the distortion in the radiation pattern is tremendous due to the current outflow on the outer shield of the coaxial cable.Second, when the balun is further away from the dipole, look at the curve $\lambda/2$. It is evident from the Fig. 5.3 by introducing the balun in the range from $\lambda/20$ to $\lambda/4$ significantly reduces this error in the radiation pattern.

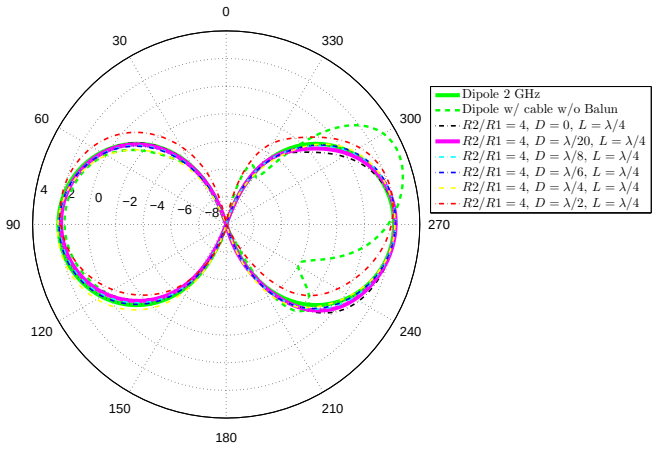

Figure 5.3: *Comparison of dipole directivity dBi at 2 GHz w/ and w/o Balun at $\phi = 90°$ cut in elevation plane.*

In Fig. 5.4 it is depicted the comparison of the reference dipole directivity in dBi at 2 GHz with and without a balun at $\theta = 90°$ and cut in azimuth plane. Repeatedly, the worst scenarios are the dipole with an infinite RF cable and with the balun of distance $\lambda/2$. Whereas, the rest of the result are in good agreement with the reference antenna.Specifically, the balun with distance of $\lambda/20$, shows max directivity at $\theta = 90°$ of 2.3 dBi, while the reference antenna has maximum gain of 2.14 dBi and this leads to an error of 0.16 dBi, which could be considered as a small error.

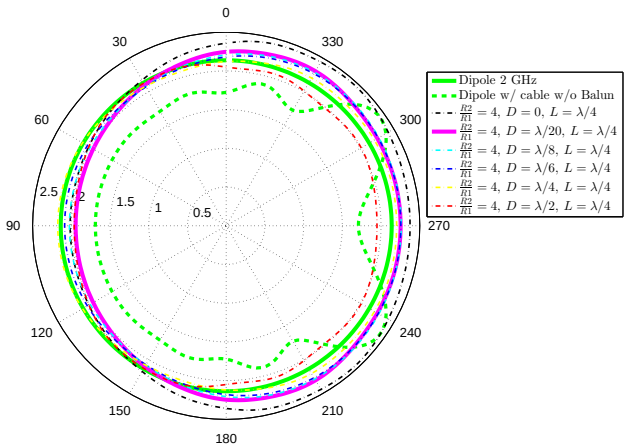

Figure 5.4: *Comparison of dipole directivity dBi at 2 GHz w/ and w/o Balun at $\theta = 90°$ and cut in azimuth plane.*

5.2 Investigation of the Ration of the Bazuka Balun

As was mention in Sec. 5.1 the best position of the balun was chosen to be at $\lambda/20$ due to the similar results as the reference antenna with regard to impedance matching and radiation pattern. Hence, in this section the investigation will be conducted with respect to the ratio of the balun recall Fig. 5.1 on page 45 and the results are illustrated in Fig.5.5. Increasing the ration leads to shifting the resonance of the antenna to higher frequency and the impedance is decreased, which will lead to higher gain.

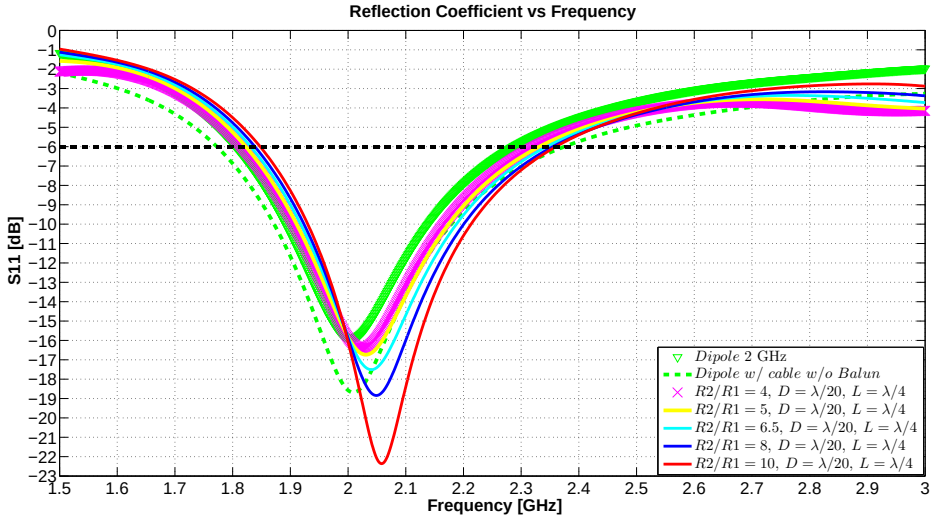

Figure 5.5: *Impedance of dipole w/ different ratios of the Balun.*

In Fig. 5.6 it is depicted the comparison of dipole directivity in dBi at 2 GHz for $\phi = 90°$ and cut in elevation plane for different ratios of the Balun. Bear in mind, that the range of the gain pattern is enormous in the range of -40 to 5 dBi and it is hard to analyze the the results, where the gain has its maximum. Hence, comparing the nulls of dipole resemblance appears at $R2/R1 = 5$ and $R2/R1 = 4$ ratios with the reference antenna; while the increasing the order of ratio of the balun, the error is higher at the nulls.

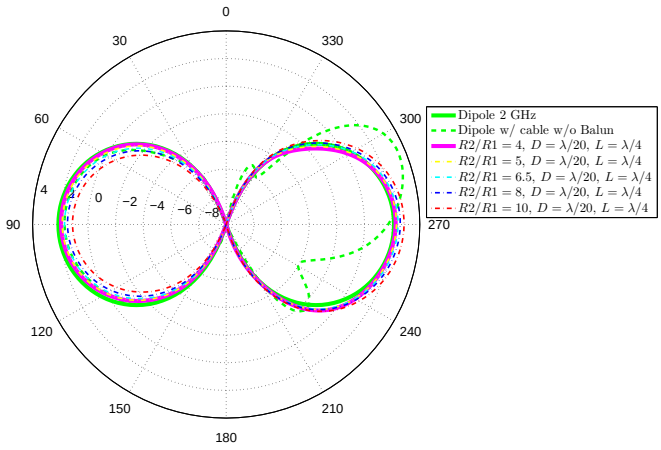

Figure 5.6: *Comparison of dipole directivity dBi at 2 GHz at* $\phi = 90°$ *and cut in elevation plane for different ratios of the Balun.*

Furthermore, in Fig. 5.7 is displayed the comparison of dipole directivity in dBi at 2 GHz at $\theta = 90°$ and cut in azimuth plane for different ratios of the Balun. Increasing the ration of the balun produce higher directivity towards the balun at $\theta = 270°$; whereas decrease it at $\theta = 90°$ and this is similar to the effect of the Yagi antenna. The gain of the $R2/R1 = 10$ at $\theta = 270°$ is 2.9 within an error of 0.76 dBi, while at $\theta = 90°$ shows an error of 1 dBi.

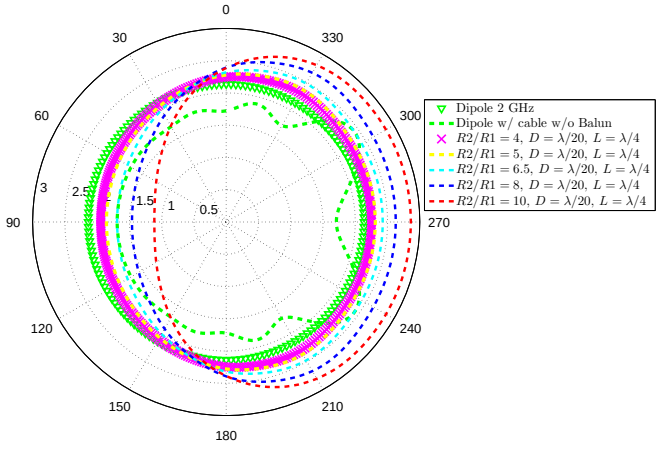

Figure 5.7: *Comparison of dipoledirectivity dBi at 2 GHz at* $\theta = 90°$ *and cut in azimuth plane for different ratios of the Balun.*

5.3 Validation of the Bandwidth of the Bazuka Balun

In papers was stated [2, 10] thatthe BW the Bazuka Balun operates at approximately of 10% of its center resonance frequency. In order to validate the BW of the balun, comparison of the radiation pattern of the reference dipole and the balun with a fixed position of $\theta = \lambda/20$ and ratio $R2/R1 = 4$ of balun will be performed. In the previous section of this chapter, the performance was evaluated at 2 GHz. Hence, in this section an evaluation will be shown only for the the lowest and highest possible frequency, where the performance is within an tolerable error. In Fig.5.8 is presented the directivity dBi at 1.9 GHz for $\phi = 90°$ cut in elevation plane. Notice that at $\theta = 270°$ the difference in directivity is of 0.8 dBi and at $\theta = 90°$, the error is 0.16 dBi.

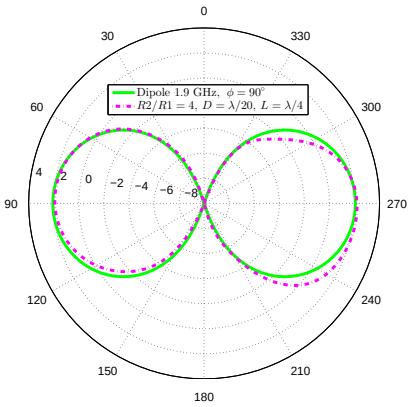

Figure 5.8: *Comparison of dipole directivity dBi at 1.9 GHz w/ Balun at* $\phi = 90°$ *cut in elevation plane.*

In addition in Fig.5.9 for 1.9 GHz is illustrated the directivity dBi at $\theta = 90°$ cut in azimuth plane, where the result in good agreement with the reference antenna.

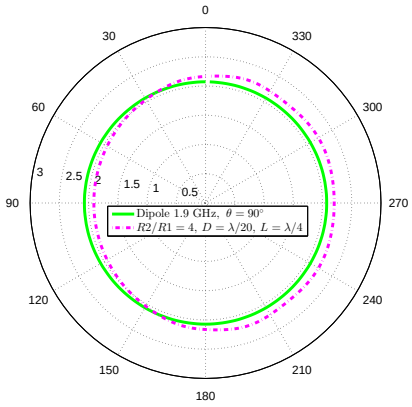

Figure 5.9: *Comparison of dipole directivity dBi at 1.9 GHz w/ Balun at* $\theta = 90^\circ$ *cut in azimuth plane.*

In Fig.5.10 is displayed the directivity dBi at 2.1 GHz for $\phi = 90^\circ$ cut in elevation plane, where the error is in an acceptable level.

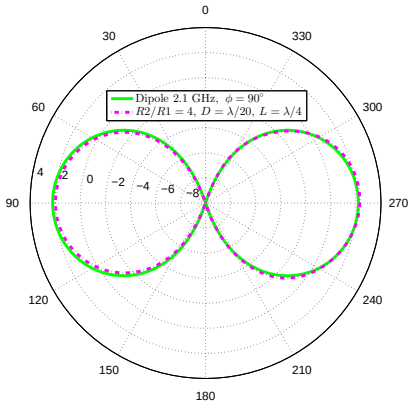

Figure 5.10: *Comparison of dipole directivity dBi at 2.1 GHz w/ Balun at* $\phi = 90^\circ$ *cut in elevation plane.*

As a final Fig.5.11 for 2.1 GHz is illustrated the directivity dBi at $\theta = 90^\circ$ cut in azimuth plane, where the result in good agreement with the reference antenna.

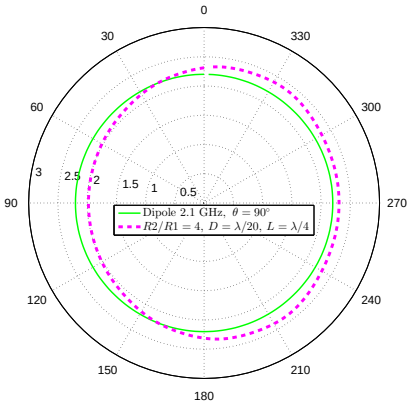

Figure 5.11: *Comparison of dipole directivity dBi at 2.1 GHz w/ Balun at* $\theta = 90°$ *cut in azimuth plane.*

As a result, it has been validated that the BW of the Bazuka Balun is approximately of 10% within the range of an acceptable error. Thus this balun will be manufactured and tested with the prototypes of the PIFA and Monopol antenna.

Chapter 6

User Effects Investigation

In this chapter are described simulation of the designed antennas in chapter **??** on page ?? and their interaction with the human hand and head. For setting up the simulation are used CTIA specifications 1.4.2 on page 4.

6.0.1 User simulation manufactured monopole antenna

As a start the antenna elements and the PCB as described in 3.2.3 on page 23 were put in a casing. It is a rectangular with 1mm thick walls and is made from the same material as the antenna carrier - Arlon ISO 933 ($\varepsilon_r = 2.33$), this geometry is shown on Fig. 6.1 on the following page. The antenna was simulate in CST only with the casing, the results for the return loss is presented on Fig. 7.7 on page 65. On Fig. 6.3 on page 55 are shown s-parameters of the simulation with the casing and MIMO mirror same side configuration, from the results it can be observed that all resonant frequencies for the simulation with the casing are shifted to the left. The reason for this is that the electric permittivity($\varepsilon_r = 2.33$) of the casing is different than the permittivity($\varepsilon_r = 1$) of the air.As it is known from physics the electric field is inversely proportional to to ε_r, therefor increase in ε_r shifts the resonant frequency to left . During simulation it was also observed that if another material with higher ε_r is used, then the frequencies are shifted correspondingly.

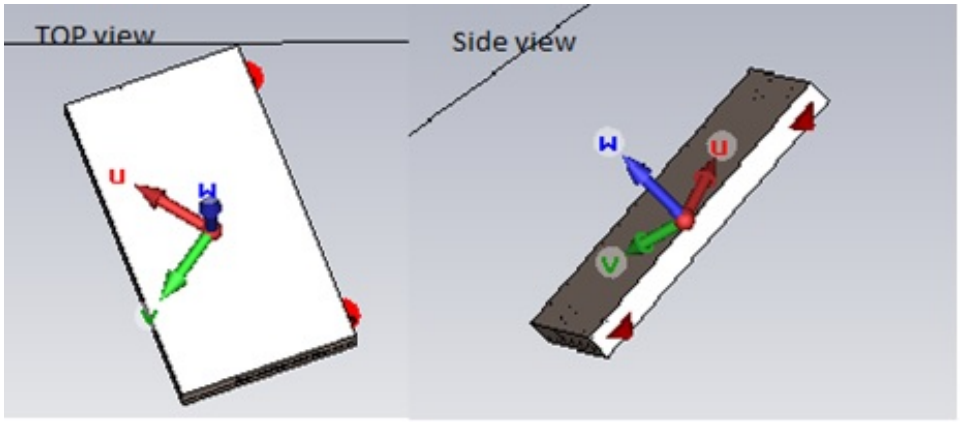

Figure 6.1: *Antenna elements inside a casing.*

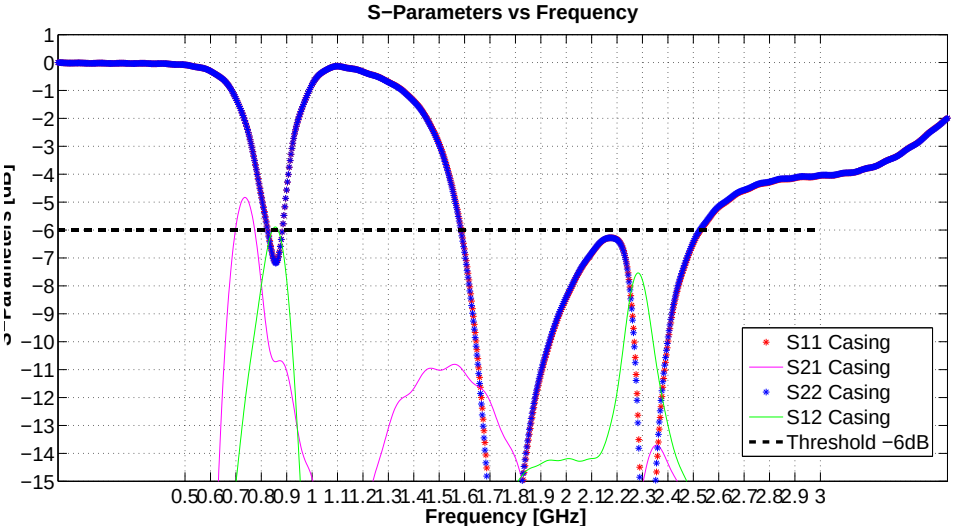

Figure 6.2: *Return loss parameters of antenna with casing.*

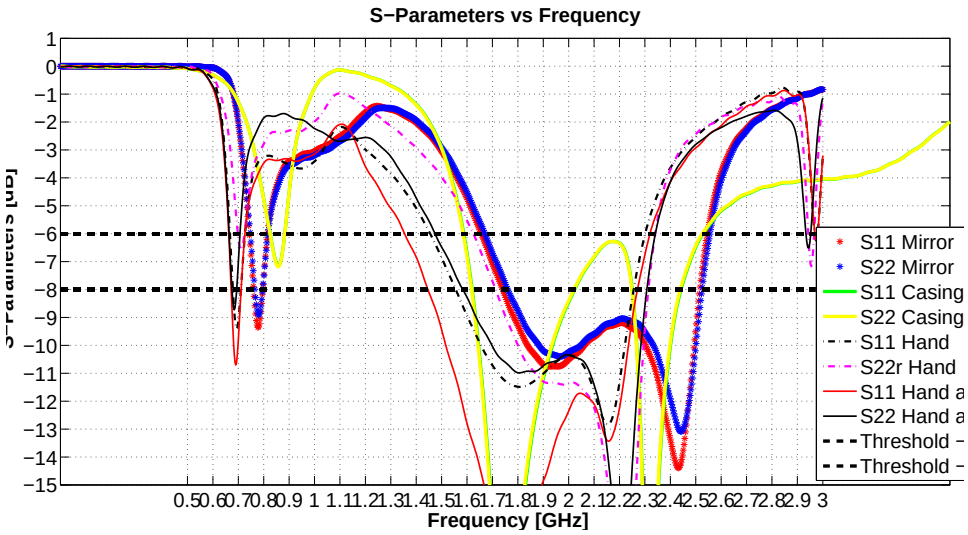

Figure 6.3: *Return loss parameters of antenna with casing, Hand simulation, Hand and head simulation.*

Once the antenna was simulated with the casing the next step is the elements to be simulated with the user hand. All requirements were kept as shown on Fig. 6.4 on the next page.The results of the return loss coefficient for the simulation with the hand are shown on 6.5 on the following page and also for comparison with the s11 and s22 parameters with the other simulations on Fig. 6.3. On Fig. 6.3 and 6.5 on the next page it can be seen that due to the hand effect the top and bottom antenna have different s11 and s22 parameters. This is due to the losses in the hand and mismatch losses. The presence of human tissue in the near field of the antenna changes the input impedance of the antenna and changes the antenna matching. In addition radiated power is absorbed in the tissue and this decrease the radiation efficiency. On Fig. 6.6 on page 57 is plotted the efficiency of the antenna, as it can be seen both antennas have lower efficiency than the simulation of the MIMO mirror and the casing simulation. Also the effects of energy absorption and mismatch losses are bigger for antenna 1, that is closer to the palm and fingers. Antenna 2 has better performance because it is in touch via the casing only with the index finger.

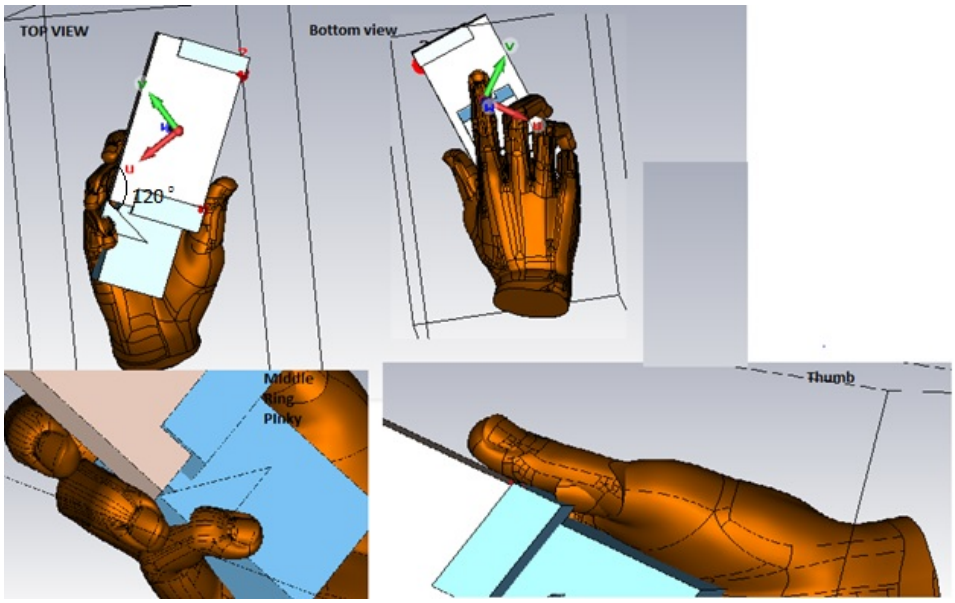

Figure 6.4: *Hand Grip as per CTIA requirments.*

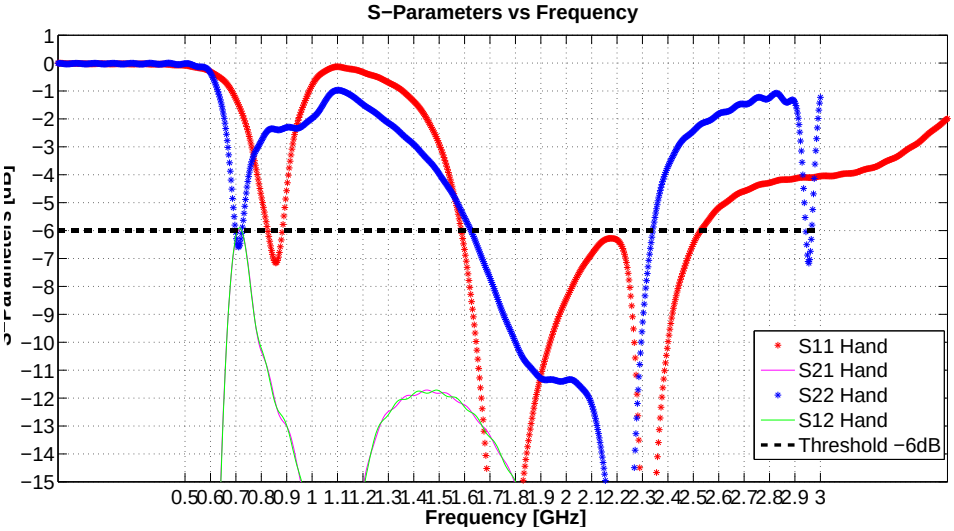

Figure 6.5: *Return loss parameters of simulation with user Hand.*

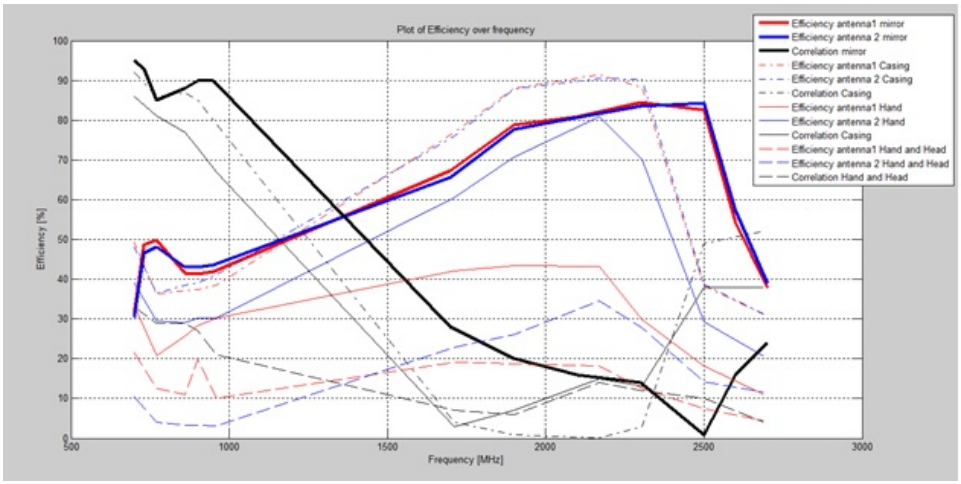

Figure 6.6: *Efficiency of original antenna, antenna with casing, hand simulation, hand and head simulation.*

Once having simulation with user hand, in this simulation was added the head in order to see how it affect the performance of the phone. It is challenging to fulfill the requirement 1.4.2 on page 4 the phone to be tilted 6° from the cheek, that's why the distance between the cheek and the EUT was measured and is 5 mm. On Fig. 6.3 on page 55 is shown the geometry of the hand and head simulation. Analyzing the results of the simulation with the head and hand shows that due to the body effect the resonant frequencies are again shifted to left as shown on Fig. 6.3 on page 55 and Fig. 7.15 on page 70. On Fig. 7.15 on page 70 is given the efficiency of the antenna, the element that is closer to the head has lower efficiency than the one that is in touch only with the hand. The efficiency of the antenna closer to the head is no more than 10% in low frequency and the highest efficiency in the high frequency is close to 35%. The efficiency of the antenna that is in the hand is almost double in the low frequency and has better performance also in the high frequency. From this simulation it is confirmed the conclusion that body tissue next to the phone seriously affects the performance of the antenna.

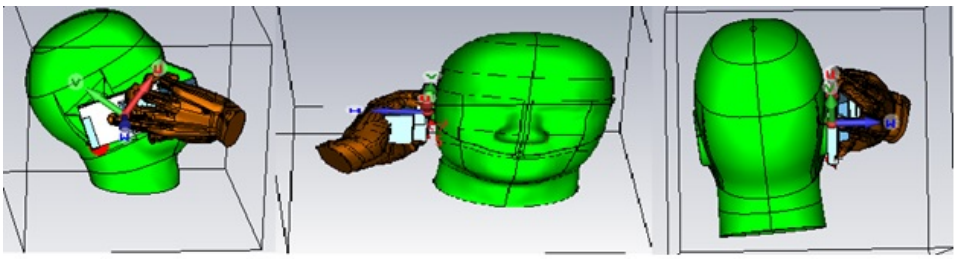

Figure 6.7: *Hand and Head as per CTIA.*

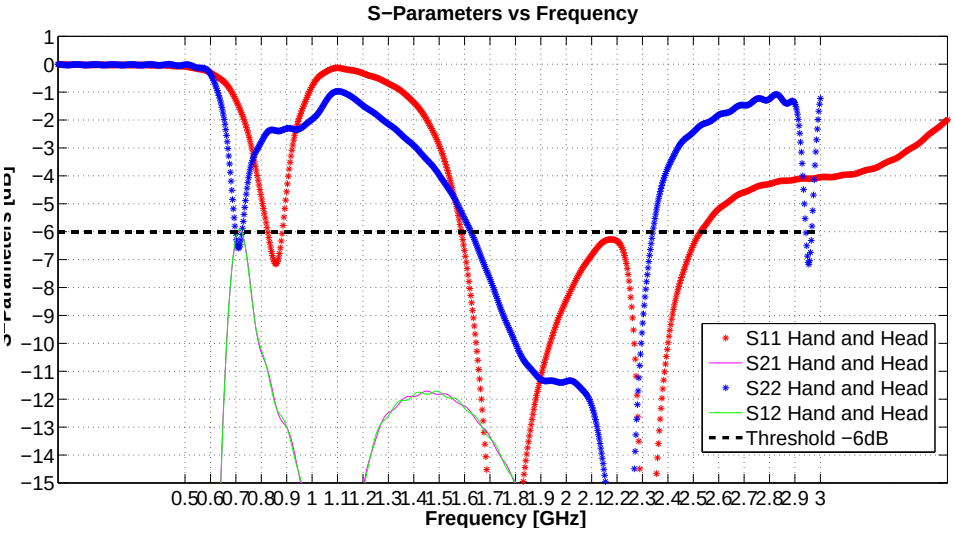

Figure 6.8: *Return loss parameters of simulation with user hand and head.*

Part II

Implementation

Chapter 7

Manufactured Monopole Antenna

In this chapter is describer the manufactured monopole antenna as simulated in 3.2.3 on page 23.

7.1 Manufactured element and casing

Final mock-up of the antenna is shown on Fig. 7.1 on the next page. The antenna prototype was measured with VNA and in an-echoic chamber. The measured return loss coefficients are shown on Fig. 7.2 on page 62. The bandwidth (VSWR 3:1) is 135 MHz. It covers frequencies from 756 MHz to 891 MHz. For the high band the bandwidth is 942 MHz, starting from 1818 MHz to 2760 MHz. When the s-parameters of the antenna are compared with the simulation 7.3 on page 62 it can be seen that there is resemblance in the low frequencies . For high frequencies of the mock-up, it is observed that they are shifted to right with approximately 140 MHz. This might be due to this how arm 1 which is responsible for this resonance frequencies is glued to the carrier. When glued it was not aligned with the carrier as in the simulation, the difference is in a couple of mm but those mm are out of the carrier and this combined with unstable gluing of this arm to the carrier leads to lower permittivity under this arm. As it is known from electromagnetic theory permittivity is inversely proportional to the electric field. So lower permittivity means higher resonant frequency. As per the simulation of the antenna and the casing described in 6.0.1 on page 55, manufactured antenna was put in a specially design casing. The casing is 1mm thick, inside is empty and with the dimensions of the antenna Fig. 7.6 on page 64. Reflection coefficients of the antenna in the casing were measured with VNA, the results are presented on Fig. 7.4 on page 63, on the same plot are presented s parameters of the antenna without casing for comparison. It can be seen that the resonance frequencies are shifted to right

in contrast with the simulation. The reason for this that the manufactured casing is not from the same material as the simulated. Permittivity of the material that was available in the lab is 2.1, in comparison with 2.33 of the simulated material, in addition in the manufactured casing has a hole so the cables can be taken away from the casing, in this area the permittivity is lower (air =1). For the purpose of the measurements with the hand and head the casing had to be done more robust in order to resist the user grip. This was achieved by adding tape on the corners for for support. On the other hand the tape has high permittivity and this affects the reflection coefficient of the antenna as shown on Fig. 7.5 on page 64. Reflection coefficient of the antenna put in the second casing is more resembled with the simulated results.

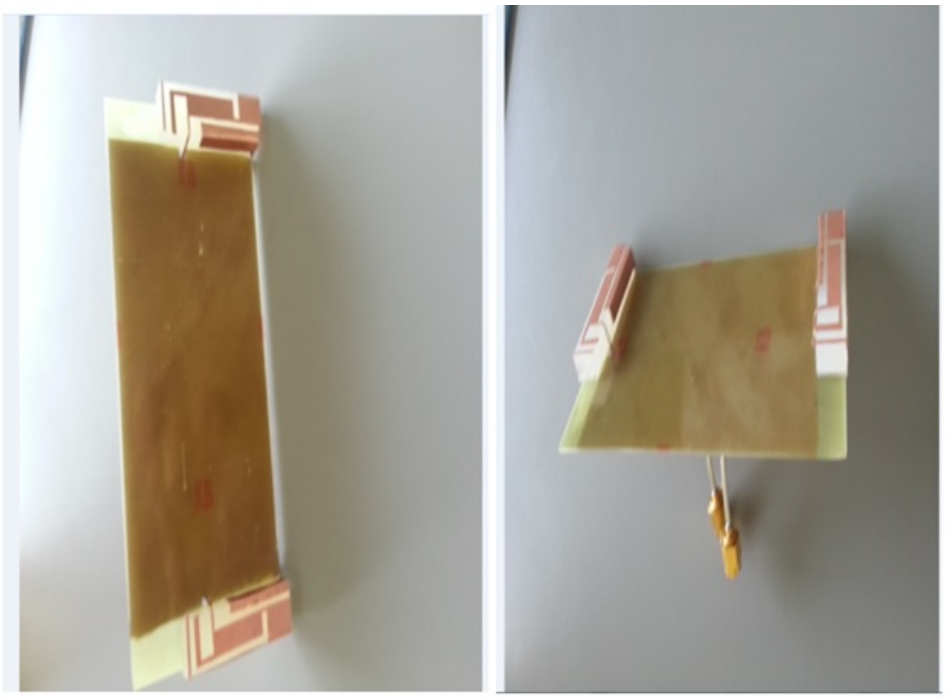

Figure 7.1: *Manufactured antenna mockup.*

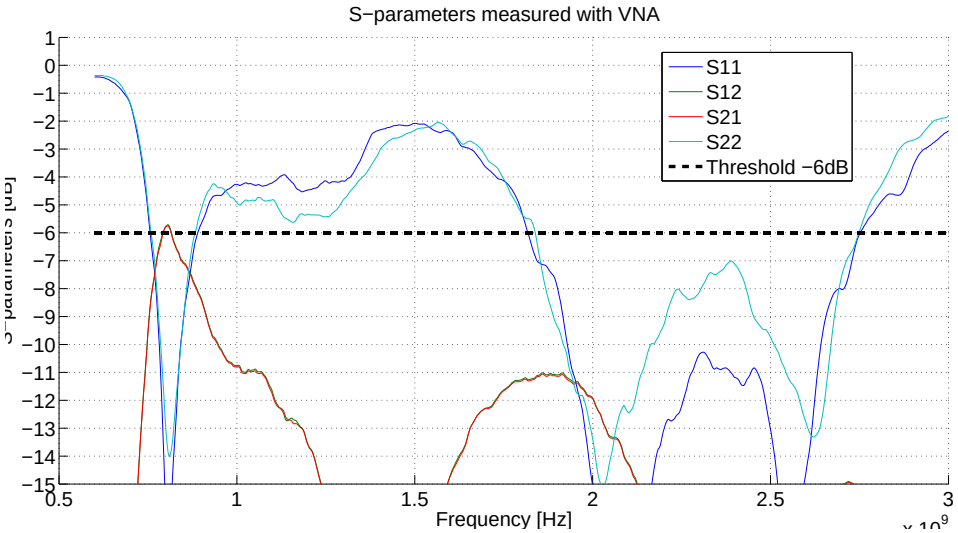

Figure 7.2: *Return loss coefficients of measured monopole antenna with VNA.*

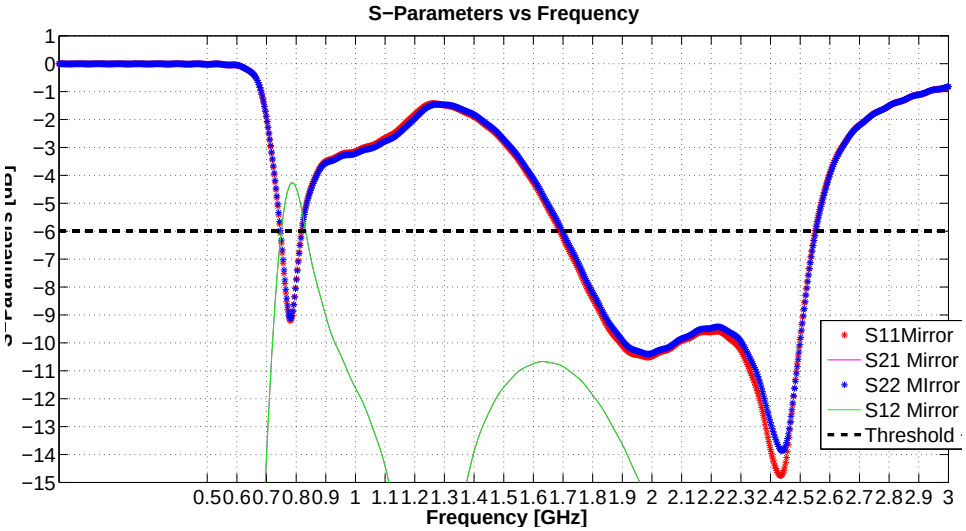

Figure 7.3: *Return loss coefficients of simulated monopole antenna MIMO mirror.*

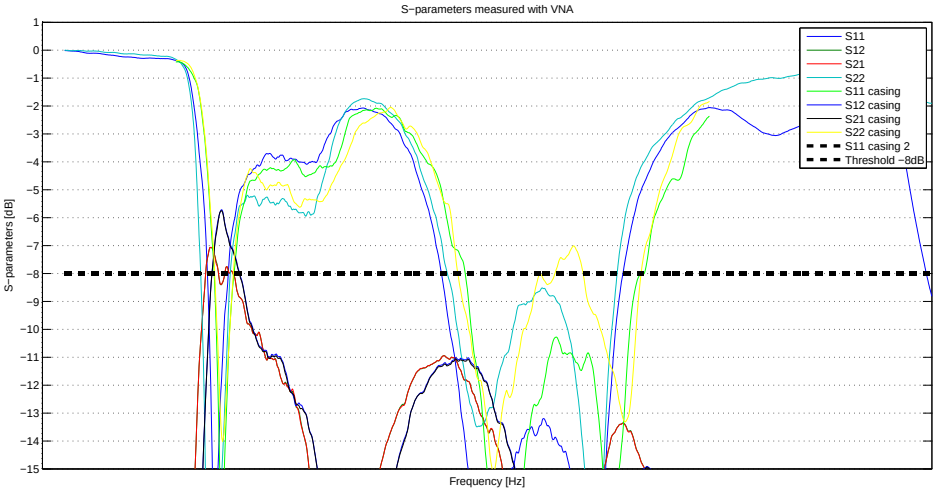

Figure 7.4: *Return loss coefficients of monopole antenna inside a casing MIMO mirror.*

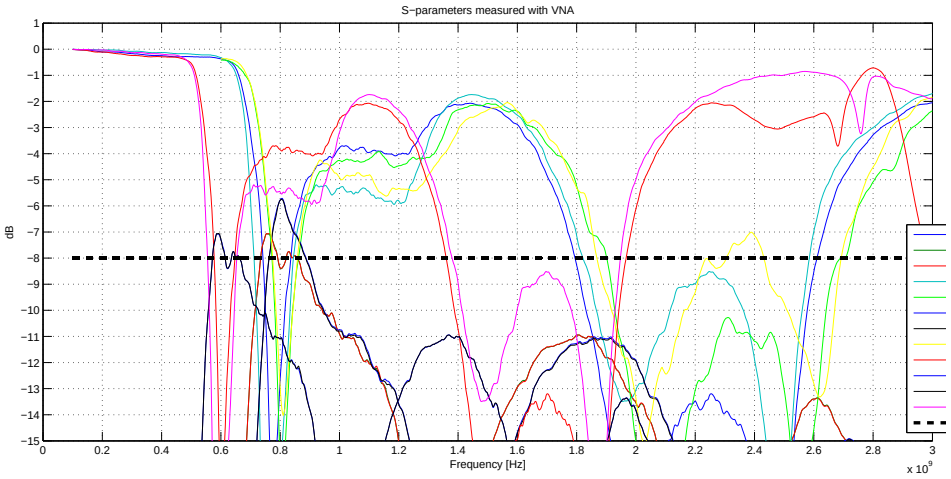

Figure 7.5: *Return loss coefficients of monopole antenna inside a casing MIMO mirror.*

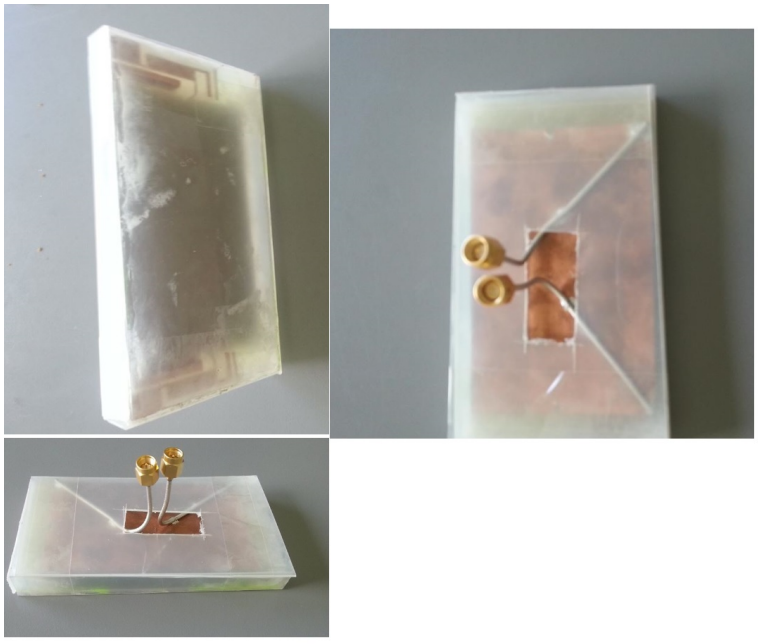

Figure 7.6: *Manufactured antenna with casing.*

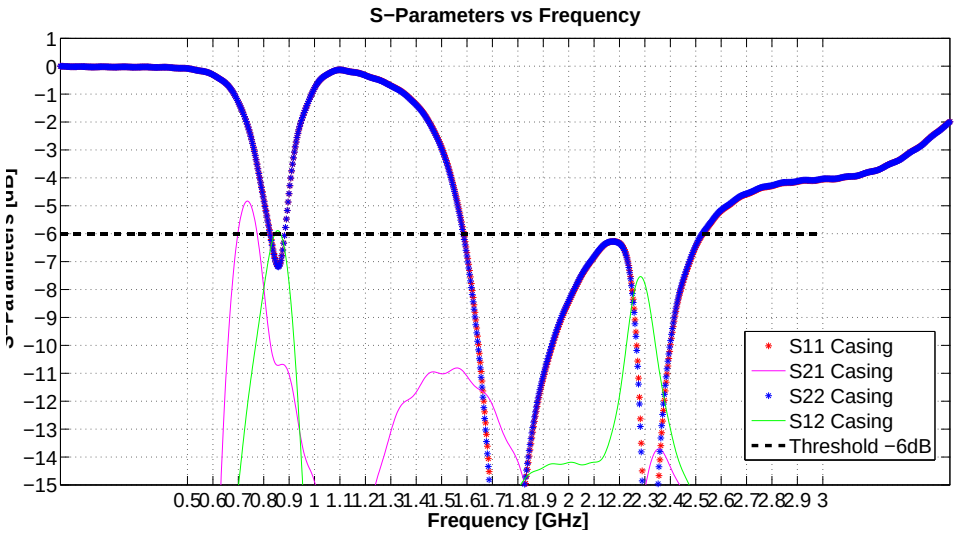

Figure 7.7: *Return loss parameters of antenna with casing simulation.*

7.2 Anechoic Chamber measurements

Manufactured antenna's efficiency was measured in anechoic chamber. Results for low frequencies are presented on Fig. 7.8 on the following page for high frequencies results are presented on Fig. 7.9 on the next page. As it can be seen by comparison of the simulated and measured efficiency results are very similar. Antenna has good efficiency from industry point confirmed from simulations and measurements. In the low frequencies in the range 700-740 MHz efficiency is a bit lower 25% -35 %, after that efficiency increase over 40 % for the all low frequencies bands, peak efficiency value in the low frequencies is 56 %. For high frequencies over 50 %, except in the interval 1.7GHz to 1.8 GHz.

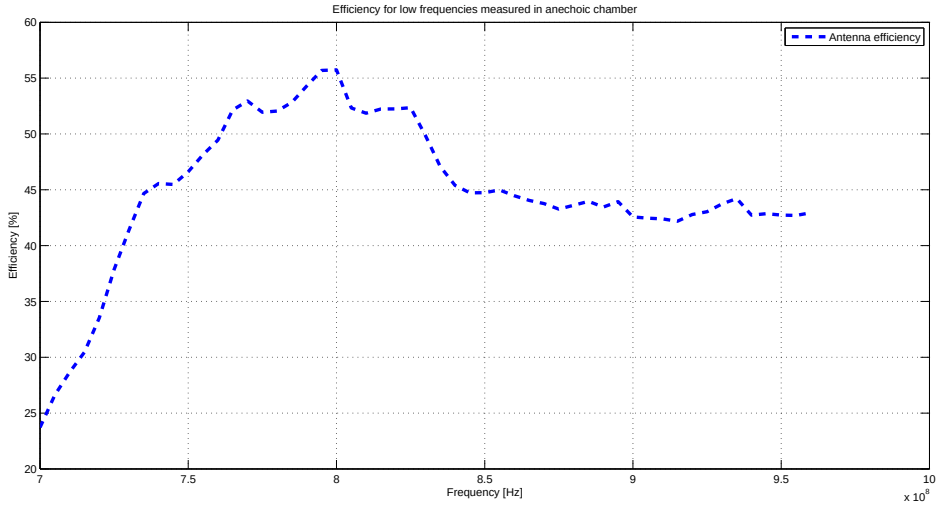

Figure 7.8: *Efficiency of antenna measured in anechoic chamber.*

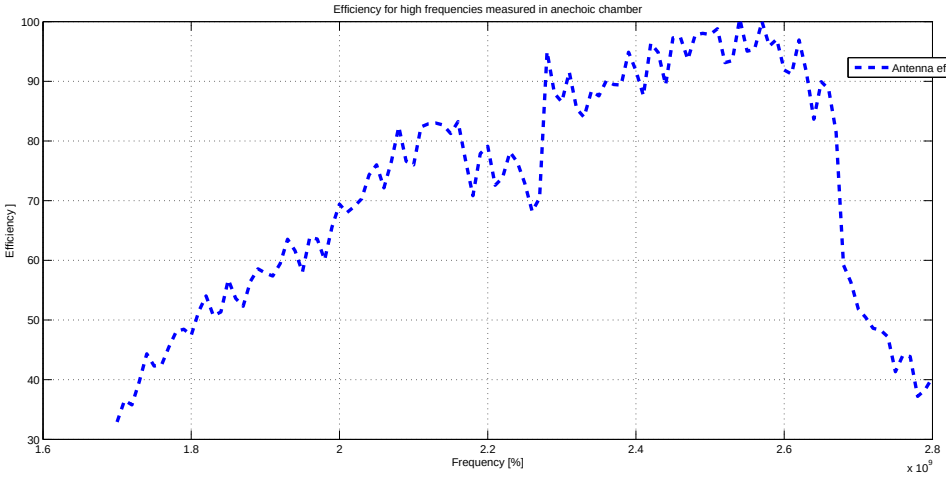

Figure 7.9: *Efficiency of antenna measured in anechoic chamber.*

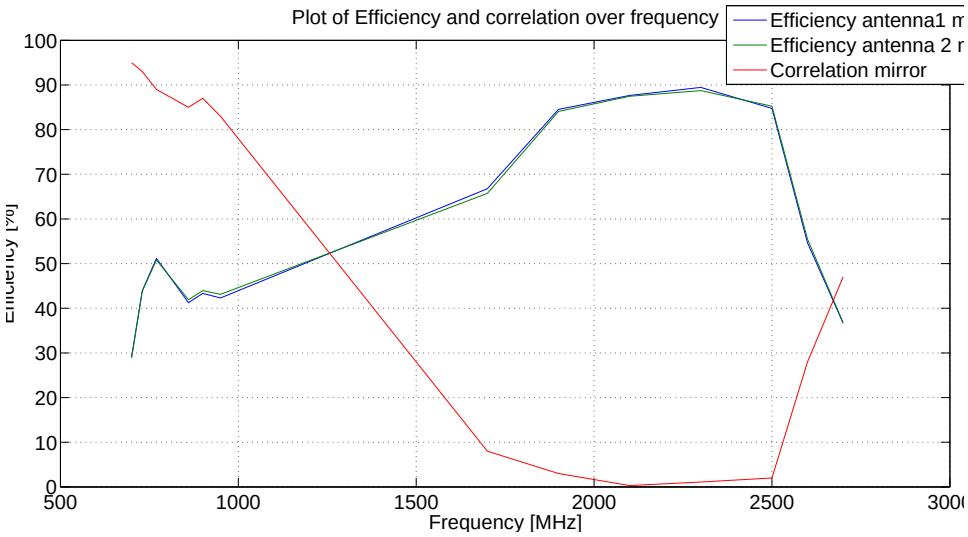

Figure 7.10: *Efficiency and correlation of MIMO mirror.*

7.3 User measurements

Measurements of the user effect was done for the antenna. Antenna with the casing was put in the hand phantom as per the CTIA requirements 1.4.2 on page 4. Phantom for devices bigger wider than 56mm was used. On Fig. 7.12 on the next page and Fig. 7.13 on page 69 is shown how the hand and the the phone are in contact. Once the setup with the hand and EUT was ready the cables of the VNA should be connected to the antenna. It was chosen position of the cables where they are plugged into the antenna from the cut in the casing and sneaked under the cheek spacer as shown on Fig. 7.11 on the next page. This position was chosen because it was analyzed that 4 on page 44 best postion for the cables is when they are in the middle of the ground bent perpendicularly. Still the expected cabel effect has to be taken into account unless measurements with choke are done. On Fig. 7.14 on page 70 are presented the reflection coefficients of the antenna measured with VNA. On Fig. 7.15 on page 70 are presented simulated s parameters of the antenna affected by the user. It can be seen that the two plots are not similar, which may be explained with the strong cable effects in the simulation.

Figure 7.11: *Cable position.*

Figure 7.12: *Grip of the EUT as per CTIA requirments.*

Figure 7.13: *Grip of the EUT as per CTIA requirments.*

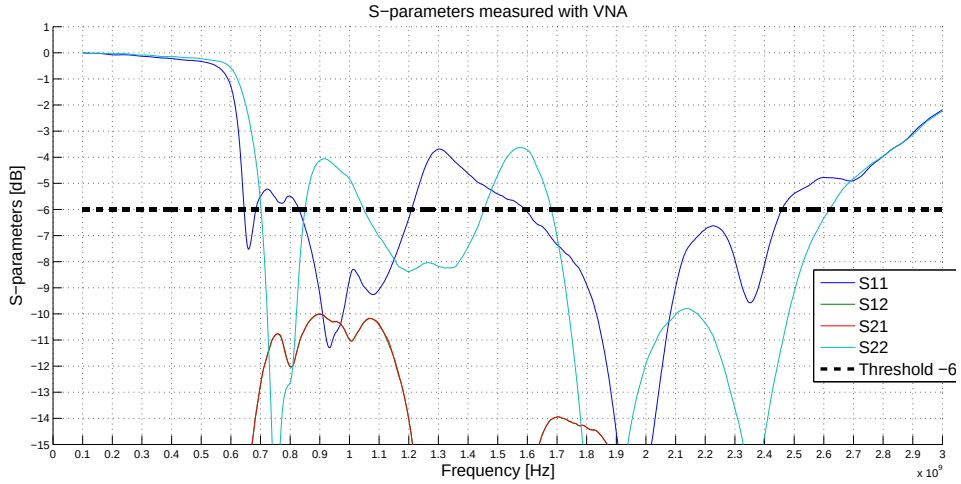

Figure 7.14: *Measurements with VNA of the hand and head effect.*

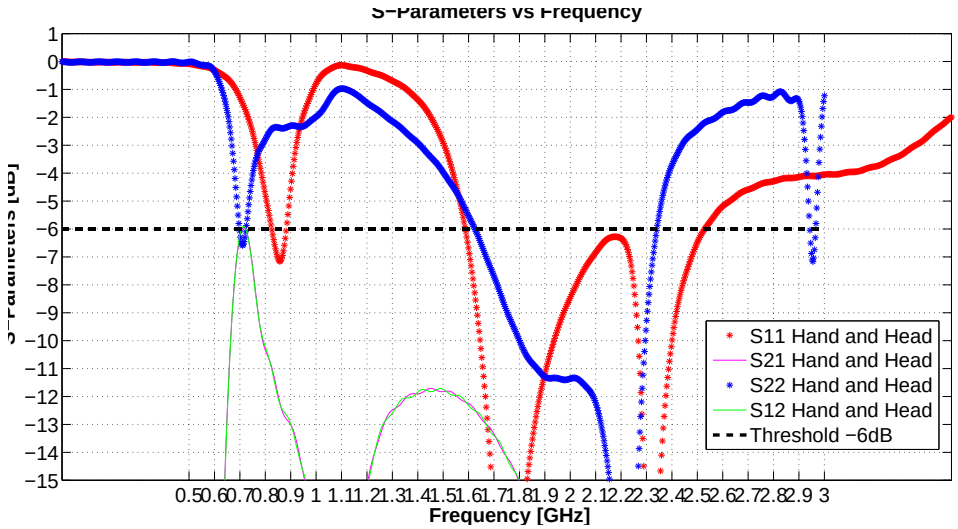

Figure 7.15: *Return loss parameters of simulation with user hand and head.*

Chapter 8

Manufactured PIFA

8.1 PIFA

Recall Sec. 3.1 on page 11, where the PIFA were fully investigated. Furthermore, in Fig.8.3 is illustrated the manufactured prototype without the casing.

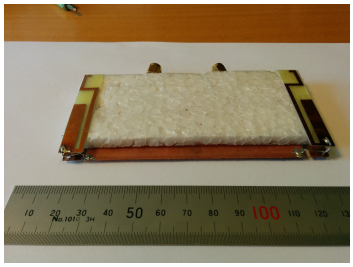

Figure 8.1: *Left side view*

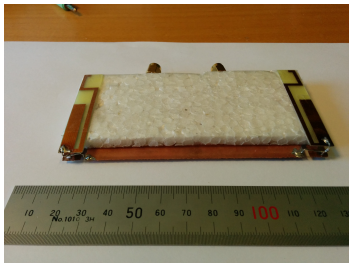

Figure 8.2: *Right side view*

Figure 8.3: *Manufactured PIFA*

In addition measurements for the S-parameters have been made with VNA for the PIFA without the casing and this is depicted in Fig. 8.4. The tag markers above the threshold level of < -6 are valid for the purple curve, whereas the makers below it are for the green curve. From the results it is seen that the reflection coefficients are not symmetric throughout the entire spectrum and the reason for it might be the cable effects and not very precisely manufactured dimensions.The low band the resonance is at 940 GHz and the aim is to put this resonance at 900 in order to cover the low band GSM900 as was simulated in Sec. 3.1 on page 11.Bear in mind that this for this prototype ware considered the casing, which will have higher dielectric constant and will shit down the resonance frequencies.

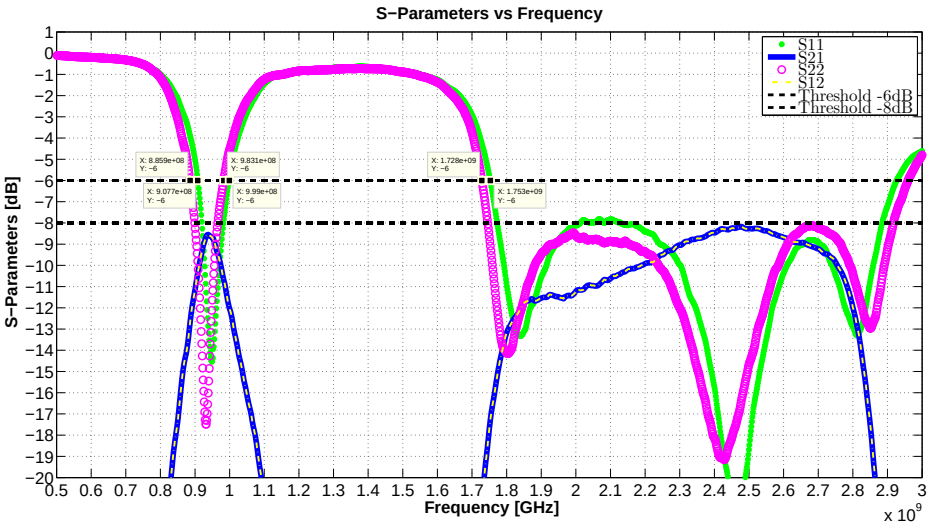

Figure 8.4: *Measured S-parameters of the PIFA w/o casing.*

In Fig. 8.5 is illustrated the PIFA plus casing. The casing is made out of ARLON recall Sec. 1.5 on page 5 and the taken S-parameter are shown in Fig. 8.6. As expected the resonance frequencies have been shifted down although the casing will make less efficient the antenna, where more energy will be dissipate as heat.

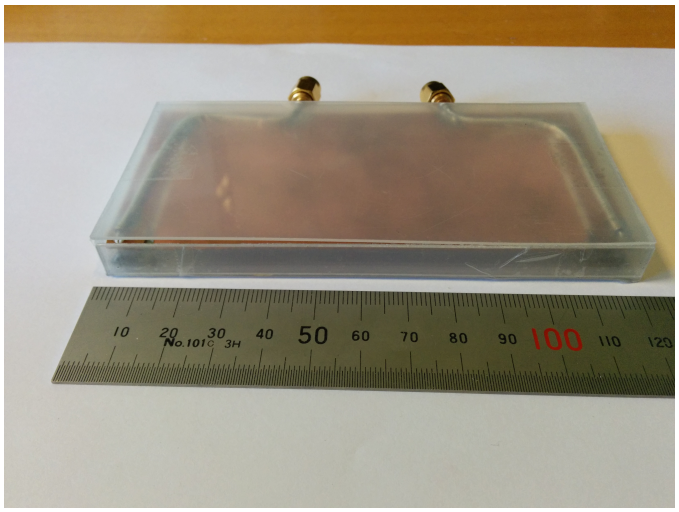

Figure 8.5: *Manufactured PIFA plus casing.*

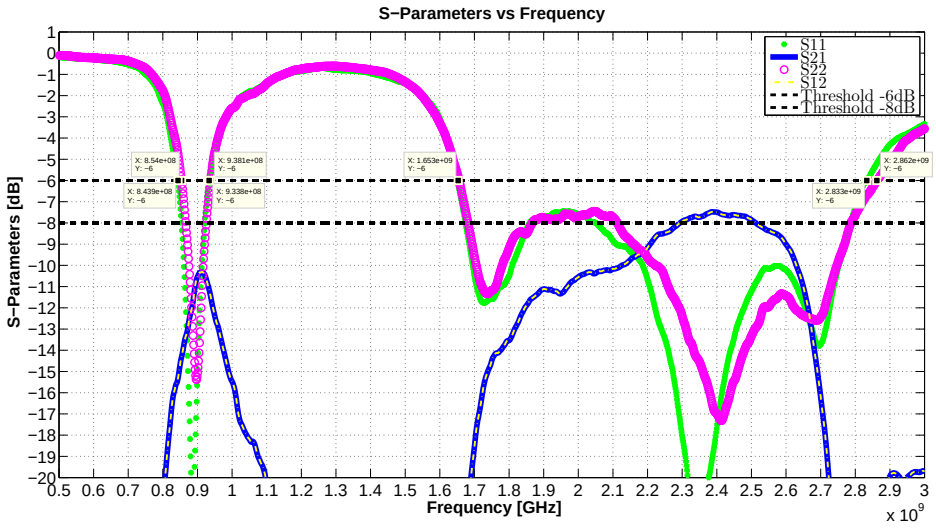

Figure 8.6: *Measured S-parameters of the PIFA w/o casing.*

Furthermore, the procedure for measuring the head plus hand was already described in Sec. 7.3 on page 67 and done the same except that for PIFA was used the hand with maximum width of the hand 56 mm and the cable position was different. In addition grip of AUT under specification of CTIA is illustrated in Fig. 8.9 and in Fig. 8.10.It is important to notice that for this set the user had a positive effect on on the performance of the antenna from the perspective of S-parameters. At the presentation more results with regards to simulation and measurements will be presented.

Figure 8.7: *Cable position*

Figure 8.8: *Side view*

Figure 8.9: *Grip of AUT under specification of CTIA*

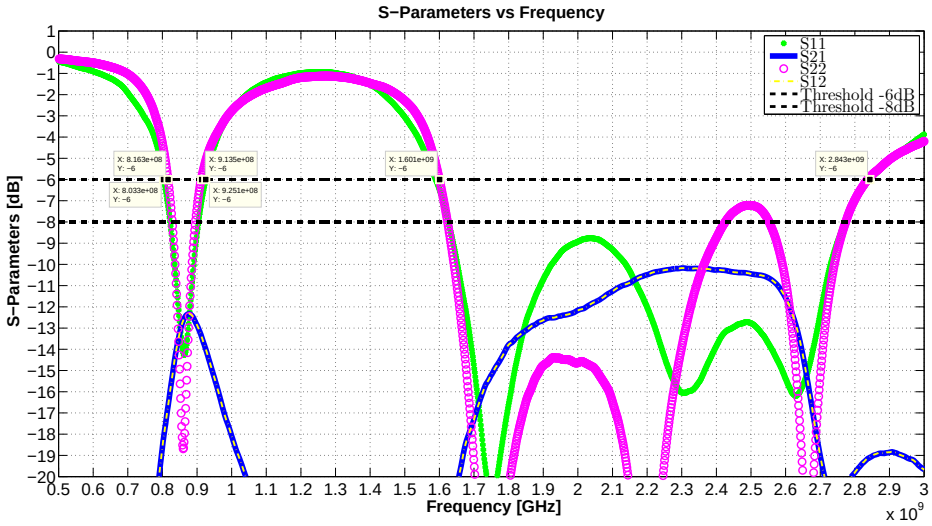

Figure 8.10: *Measured S-parameters of the PIFA w/o casing, head and hand.*

Bibliography

[3] Y.-L. Ban and J. L.-W. L. Jin-Hua Chen, "Small-size printed coupled-fed antenna for eight-band l te/gsm/umts wireless wide area network operation in an internal mobile handset," 2013.

[1] B. Z. Ying, "Antenna Cellular Phones for Mobile Communications," 2012.

[2] C. Icheln, J. Krogerous, and P. Vainikainen, "Use of balun chokes in small-antenna radiation measurements," 2013.

[4] J. Anguera, A. Cabedo, and C. Picher, "Multiband hanset anennas by means of groundplane modification," 2007.

[5] ——, "Multiband hanset anennas combining pifa, slots, and ground plane modes," 2009.

[6] Y.-J. Ren, "Ceramic based small lte mimo handset antenna," 2013.

[7] W. Yu, S. Yang, and M.-H. Cho, "A new multi-band diversity antenna used for mobile phone," 2009.

[8] M. I. Chan-Woo Yang, Young-Bae Jung and I. Chang Won Jung, Member, "Octaband internal antenna for 4g mobile armset," 2013.

[9] I. R. M. L. F. I. F. L. Z. L. M. I. J. J. Qingxin Guo, Senior Member and J. Byun, "Interaction between internal antenna and external antenna of mobile phone and hand effect," 2013.

[10] S.A.Saaria, J. Lu, and D. Thiel, "Full-wave analysis of choking characteristics of sleeve balun on a coaxial cables," 28.0.3.2002.